THE ASTROPHYSICAL JOURNAL, 374:150–168, 1991 June 10

VARIABILITY OF INTERSTELLAR HYDROXYL MASERS

ANDREW W. CLEGG[1] AND JAMES M. CORDES
Department of Astronomy, Space Sciences Building, Cornell University, Ithaca, NY 14853
Received 1990 August 6; accepted 1990 December 5

ABSTRACT

The spectra of 10 interstellar OH maser complexes were monitored in the 1665 MHz transition for variability on short (minutes–hours) and long (days–years) time scales. Eight of the sources exhibit short time scale variability in the relative amplitudes of the spectral features above that expected due to radiometer noise, and all sources for which multiepoch observations were made show variability on long time scales. Amplitudes of the short time scale fluctuations are typically 5%–10% of the peak intensity and are as large as 20%. Over long time scales, the fluctuations range from 0 to nearly 100% in amplitude. The OH emission spectrum from a main-line OH/IR star was also monitored. Long time scale variability is noted, distinct from that caused by pulsations of the stellar pumping source, while no short time scale variability (above 5%) is apparent. The origin of the short time scale fluctuations of the interstellar masers is not clear. Instrumental effects are unlikely. The variability is either propagation-induced (interstellar scintillation), or intrinsic to the masers. Scintillation requires angularly compact sources with exceedingly large brightness temperature approaching 10^{24} K. Alternatively, the variations are the response of the masers to a series of pump disturbances, or fluctuations of the masing level populations about their steady-state values. Brightness temperatures of 10^{10}–10^{15} K are implied, depending on the true nature of the maser light curves for which we have only a small time sample. The long time scale variability is likely an intrinsic property of the masers.

Subject headings: interstellar: molecules — masers — radio sources: variable

1. INTRODUCTION

Interstellar H II/OH masers are intriguing sources associated with early stages of star formation (Reid & Moran 1988). The masers are found on the edges of expanding H II bubbles surrounding newly formed stars. Individual maser spots have been localized using VLBI observations to regions no larger than 7 AU in size (Diamond et al. 1988).

The VLBI results are upper limits to the angular sizes of the emission regions—the images of the masers may be smeared by the effects of interstellar scattering, where the radiation is diffracted by electron density irregularities in the interstellar medium. This interpretation was suggested by Burke et al. (1968) when VLBI results indicated a $\sim\lambda^2$ scaling in observed angular sizes of 18 cm OH and 1.3 cm H_2O masers. Furthermore, the observed angular sizes of maser spots show a tendency to increase with distance, strengthening the argument for interstellar scattering effects. Alternatively, some authors suggest that the amplitude of electron density fluctuations along the lines of sight to the masers is insufficient to explain the degree of broadening (cf. Boyd & Werner 1972), and hence the VLBI observations have in fact resolved the true (intrinsic) angular extent of the emission region. The electron density fluctuation amplitudes, however, were calibrated from scattering of emission from nearby pulsars, and were probably underestimated.

We have used the Arecibo[2] and Very Large Array[3] radio telescopes to investigate temporal and spectral variations in the output of 10 H II/OH masers in an attempt to determine their intrinsic physical properties. The observational strategy is analogous to that used in the acquisition of pulsar dynamic spectra (intensity as a function of time and frequency), in which interstellar propagation effects induce characteristic modulations (interstellar scintillation, ISS) through constructive and destructive interference of the scattered radiation (cf. Rickett 1990). If the unscattered image of the source is sufficiently large in angular extent, purely destructive or constructive interference is quenched, and scintillations are not observed. The presence of ISS therefore allows limits to be placed on the intrinsic angular size of the source.

Alternatively, if the fluctuations in time and frequency are not ISS effects, they constrain the physical dimensions of the emitting regions through travel time arguments and provide information on the pumping mechanism responsible for the existence of the masers.

Previous authors have reported variability in the spectra of H II/OH masers on time scales of years, months, and, in a small number of cases, weeks and days (cf. Sullivan & Kerstholt 1976; Weaver, Dieter, & Williams 1968). The results of these surveys are not always consistent—spectral features that are claimed to be variable by one account may not be classified as such by another. A complicating factor is the use by some authors of the combined observations of many observers, where the data have been obtained at several epochs using different telescopes, spectral resolutions, calibration schemes, polarizations, and LSR velocity origins (important in cases when the spectral lines are significantly less than a single spectral bin in width). The authors of such papers have taken great care in self-calibrating the collection of spectra, and the results are generally convincing; however, from our own experiences using identical observing set-ups over time scales of days, we know that absolute calibration is very difficult at best.

[1] Postal address: Code 4213AC, Naval Research Laboratory, 4555 Overlook Avenue SW, Washington, DC 20375.

[2] The Arecibo Observatory is part of the National Astronomy and Ionosphere Center, which is operated by Cornell University under cooperative agreement with the National Science Foundation.

[3] The Very Large Array is part of the National Radio Astronomy Observatory, which is operated by Associated Universities Inc., under contract with the National Science Foundation.

In this paper, we present sensitive observations with high resolution in time and frequency that establish the existence of fluctuations in the emission from H II/OH masers on time scales of minutes and hours and demonstrate the presence of variability on longer time scales of days, weeks, and months.

2. OBSERVATIONS

The interstellar OH masers were observed in the OH transition frequency, taken to be 1665.402 MHz. Table 1 lists the sources and their distances, the pointing coordinates used in the survey, and the velocity resolution employed at each epoch. As a control source, we monitored one stellar (OH/IR) source, U Herculis. The emission from stellar masers arises from an extended shell (Bowers et al. 1980; Sivagnanam et al. 1988), and ISS effects are likely quenched for most line components. Fluctuations in the spectrum of OH/IR sources are expected to be limited to those imparted by variability of the central star (Gómez Balboa & Lépine 1986). The optical period of U Her is approximately 400 days; thus, it can be used to probe instrumentally derived short time scale variability.

Arecibo and the Very Large Array were used to obtain dynamic spectra so that the results from two systems of very different design could be compared to further identify instrumental effects. Here we discuss the observing procedures used at each telescope, and the uncertainties involved in data acquisition.

2.1. *Arecibo*

We employed the 305 m Arecibo dish at four epochs: 1988 April (referred to as epoch 1), 1988 October (epoch 2), 1989 September (epoch 4), and 1990 March (epoch 5). The 1989 September observing epoch was abbreviated due to a hurricane. Data were obtained using the 18 cm dual circular feed with a beamwidth (FWHM) of approximately 3'.0. Dynamic spectra of the right- and left-hand circularly polarized emission were acquired simultaneously.

The received electric fields were digitized using three-level sampling, then introduced into the 2048 channel autocorrelator spectrometer. During the first two epochs, 512 lag channels per polarization were employed. The autocorrelations were accumulated for 16 s, then written to tape. After a dead time of 2 s, a new integration was begun. Off-line, the individual autocorrelations were corrected for three-level sampling and Fourier-transformed to produce power spectra. For the later epochs, 1024 lag channels per polarization were used, and the integration time was 32 s. During a 16 s dead period between scans, the data were corrected and Fourier-transformed, and the resultant power spectra written to tape. On-source time at all epochs ranged from 15 minutes to over 2 hr, depending on the source declination. Sensitivity for a 16 s integration, using a typical velocity resolution of 0.11 km s^{-1}, was $\sim$80 mJy per spectral bin. Many maser features are greater than 100 Jy in flux density, allowing signal-to-noise ratios in a single integration often exceeding 10^3.

During the observations of 1988, no real-time correction was performed for the acceleration of topocentric velocity with respect to the local standard of rest. The time-dependent velocity corrections were performed later by Fourier-transforming the power spectra, applying phase shifts, and inverse transforming, in a manner which constrained sharp spectral features from drifting throughout the observation. In all cases, the correction was less than a shift of 1.5 bins per dynamic spectrum but is important in removing fluctuations due to binning effects. In 1989 September and 1990 March, LSR velocity corrections were computed at the beginning of each 32 s integration; the observing frequency was appropriately modified in real time, and no further corrections were necessary. Velocity resolution varied with observing epoch and source. We have tabulated the various parameters in Table 1.

To obtain the highest sensitivity and time resolution possible, no absolute flux density calibration was attempted during most of the 1988 observations. However, relative calibration among individual spectra of a given polarization for a given source was constant, because signal attenuation settings and threshold levels for three-level sampling remained fixed throughout the observation. For convenience, the dynamic spectra were later normalized so that the average flux density of the brightest velocity feature was unity. During the 1989/1990 epochs, absolute flux density calibration was achieved by periodically activating in-line calibrator noise diodes. The line emission was calibrated against the noise diodes, whose equivalent flux densities were subsequently referenced to a set of extragalactic sources from the VLA calibrator manual (Perley 1982). The chosen sources exhibited flux densities that could be

TABLE 1

SOURCES AND OBSERVING PARAMETERS

SOURCE	D (kpc)	α(1950)	δ(1959)	ΔV (km s^{-1}) Epoch 1	Epoch 2	Epoch 3	Epoch 4	Epoch 5	REFERENCES
S269	2.0	$06^h11^m46^s.5$	13°50'40"	...	0.055	...	0.11	0.11	1, 2
U Her[a]	0.5	16 23 36.0	19 00 17	0.44	0.22	...	...	0.11	3
NGC 6334F	1.7	17 17 32.228	−35 44 03.60	...	...	1.1	...	...	4, 5
W49N	14.0	19 07 49.763	09 01 14.88	0.22	...	1.1	...	...	6, 5
W49S	14.0	19 07 58.0	09 00 04	...	...	...	...	0.11	6, 5
G43.8	2.7/11.8[b]	19 09 30.8	09 30 46	...	0.11	...	...	0.11	7
G45.1	10.0	19 11 00.4	10 45 44	...	...	...	...	0.11	8, 9
G45.5	10.0	19 12 04.4	11 04 15	...	...	...	...	0.11	8, 9
W51	7.0	19 21 09.8	14 24 36.5	...	...	1.1	...	0.11	6, 5
ON 1	3.5	20 08 09.8	31 22 40	0.11	...	...	...	0.11	10
W75S	2.0	20 37 14.2	42 12 12	...	...	1.1	...	...	11, 12

[a] OH/IR star.

[b] Distance to G43.8 is ambiguous.

REFERENCES.—(1) Turner 1971; (2) Wynn-Williams, Werner, & Wilson 1974b; (3) Engels 1979; (4) Neckel 1978; (5) Gaume & Mutel 1987; (6) Mezger & Höglund 1967; (7) Matthews et al. 1978; (8) Wynn-Williams et al. 1971; (9) Goss et al. 1973; (10) Hardebeck 1972; (11) Habing et al. 1974; (12) Norris et al. 1982.

described to a good approximation in terms of a simple power law in wavelength. The appropriate 18 cm flux densities were interpolated from the cataloged 20, 6, and 2 cm values. The calibrators and their adopted 18 cm flux densities were: 0406+121, 0.92 Jy; 0518+165, 8.04 Jy; 0722+145, 0.84 Jy; 1743+173, 1.10 Jy; 2032+107, 1.02 Jy; 2136+141, 1.30 Jy. The calibrator sources were assumed to possess no intrinsic circular polarization.

Off-source scans were used for baseline calibration of the spectra. For the 1988 observations, the scans were obtained by slewing off source before, after, and once during the acquisition of a dynamic spectrum for each source. For the later epochs, we employed frequency shifting, where the IF mixer frequency was modulated to place the OH line emission alternately in the lower and upper halves of the passband. Because the line emission always appeared in the passband, the two resultant spectra were used to calibrate each other, then inverted and folded on to one another, thereby recovering 100% of the integration time.

2.2. *VLA*

VLA observations were made during a seven hour period in 1989 May (≡ epoch 3). The array was in a B/C hybrid configuration, which yielded a synthesized beam size (FWHM) of approximately $5'' \times 15''$. Two maser sources previously observed with the Arecibo telescope were reobserved with the VLA. In addition, dynamic spectra were obtained for two masers which are not within the Arecibo declination range. A hardware malfunction prevented the acquisition of dynamic spectra of the OH/IR source U Her and of other potentially interesting interstellar masers.

Auto- and cross-correlations among individual array antennas were accumulated for one integration period (30 s) and written to tape. As in the Arecibo observations, the data were three-level sampled before correlation. Total on-source time was typically 40 minutes. Separate data were obtained for left and right circularly polarized emission. A total of 128 spectral channels was used across a bandwidth of 0.78125 MHz, providing a velocity resolution of 1.1 km s^{-1}. On-line Hanning smoothing was invoked to reduce "ringing" due to the presence of bright, narrow spectral features.

Between observations of masers, standard VLA calibration sources were observed and later used for amplitude and phase calibration of the *uv* visibilities. The flux densities of the calibrators were referenced to our primary calibrator, 3C 286, which was assumed to have an 18 cm flux density of 13.6 Jy. Data calibration was performed using standard NRAO software; relative phases across all baselines were adjusted for the calibrator source data (assumed pointlike in morphology), and the time-dependent corrections applied to the program sources.

Spectra were obtained from the vector sum of cross correlations among all telescope baselines. Each spectrum represents the emission contained within one synthesized beam of the array phase center. The coordinates used in the VLA survey were taken from published VLA observations with greater angular resolution, or from published VLBI data.

A limited number of sky images were created from the *uv* data using the Astronomical Image Processing System (AIPS) to verify source positions and to check for sidelobe contamination and interference.

The theoretical signal-to-noise ratio for a single bin is $S/N \simeq 18F$, where F is the maser flux density (in Jy) contained within the bin. The ratio is calculated using system parameters given by Napier & Crane (1982). Many individual maser line components possess flux densities exceeding 100 Jy, allowing S/N approaching 2000.

There are several advantages and at least one disadvantage to using the VLA over Arecibo for acquisition of maser spectra. First, the synthesized beam of the VLA is much smaller than the single-dish beam of Arecibo, which allows better isolation of maser emission within regions containing several maser complexes (e.g., W49 and W51). Additionally, usable zenith-angle coverage is much greater with the VLA. As pointed out earlier, the use of a system of different design also helps to better identify instrumental effects.

We note that there are limitations of the VLA which hamper the study of maser variability. Specifically, the limited velocity resolution of 1.1 km s^{-1} is much broader than typical maser features and, perhaps more importantly, is greater than the typical spacing between features in a given spectrum. Furthermore, only a single epoch of VLA data is available, which limits our ability to identify repeatable zenith angle– or parallactic angle–dependent instrumental artifacts. The VLA spectra are included for completeness, but we emphasize the multiepoch, high-resolution Arecibo data.

2.3. *Uncertainties*

2.3.1. *Short Time Scale*

There are numerous instrumental effects that impart short time scale variability in the spectra. We have identified, constrained, and/or eliminated most of them. These effects as they pertain to our Arecibo and VLA observations are discussed in the Appendix. The wide range of behavior observed in the Arecibo dynamic spectra is summarized in § 7 of the Appendix, where we attempt to establish that no consistent explanation of the observed variability can be obtained from instrumental effects.

2.3.2. *Long Time Scale*

Absolute flux density calibration between epochs is very difficult due to instabilities in calibrator noise sources, and variability in the flux density of extragalactic reference sources. We have attempted to minimize errors by using several extragalactic objects as flux density calibrators. Based on relative amplitude measurements of calibrator noise diodes, extragalactic sources, and system temperatures with the Arecibo telescope, we believe that the absolute calibrations are accurate to no better than 10%. We circumvent calibration errors at this level by concentrating on variability of the *relative* amplitudes of line components within a spectrum. Fluctuations that are positively correlated across all line components are discounted unless significantly greater than any plausible calibration uncertainty.

The presence of exceedingly bright line radiation poses problems for absolute VLA flux density calibration. The effect is due to referencing narrow-band correlations at the telescope back end to system temperatures obtained by wide-band measurements at the front end (cf. Rots 1982). The result is an underestimate of the narrow-band flux density. The observations presented here have not been corrected for this effect, and therefore the derived VLA flux densities may be low. However, because the maser sources are completely unresolved on all baselines, the effect is not frequency-dependent and therefore cannot produce changes in the relative amplitudes of line components for a given maser region. Again, we rely only on

changes in the line *shape* and do not make any claims about variability through comparison of absolute flux densities.

3. ANALYSIS

Our main goal is to study spectral variations on short and long time scales. Short time scale fluctuations are those evident during the acquisition of a single dynamic spectrum and occur over time scales of 16 s to 2 hr. Long time scale variations are those that occur over days, weeks, months, and/or years.

Uncertainties in absolute calibration between observing days or epochs necessitate using different methods for ascertaining the type and degree of variability on short and long time scales. In the following sections, we describe the methods used for the detection and analysis of spectral fluctuations on both time scales.

3.1. *Short Time Scale Variability*

3.1.1. *Quantification*

The observed dynamic spectrum is the frequency and time dependent flux density $F(v, t)$. In the data presented here, the continuum flux density contributions from the source and receiving system have been removed, so that $F(v, t)$ describes the spectral and temporal structure of the OH line emission.

To quantify short time scale variability of the dynamic spectrum, we define the *modulation index*, $m(v)$, as

$$m(v) \equiv \left[\frac{\langle F^2(v, t)\rangle - \langle F(v, t)\rangle^2}{\langle F(v, t)\rangle^2}\right]^{1/2}, \quad (1)$$

where the angular brackets denote time averages over the duration of the dynamic spectrum.

There are two components to the observed modulation index: a contribution due to processes intrinsic to the masers themselves or induced by propagation effects; and an additional contribution imparted by radiometer noise. Quantification of the former requires estimation and removal of the latter. The contribution due solely to radiometer noise is

$$m_r(v) = \alpha[1 + F_r/\langle F(v)\rangle](\Delta v \tau)^{-1/2}, \quad (2)$$

where F_r is the flux density corresponding to the system temperature in the absence of any line emission, $\langle F(v)\rangle$ is the mean flux density in bin v, Δv is the single-bin bandwidth, τ is the integration period for one spectrum, and α is the correction factor for three-level sampling, $\alpha = 1.51$ (Hagen & Farley 1973).

We quantify the component of the observed modulation index $m(v)$ due to effects other than radiometer noise by constructing the *modulation excess*, $m_e(v)$, defined by

$$m_e(v) \equiv \frac{m(v) - m_r(v)}{m_r(v)}. \quad (3)$$

The uncertainty in m_e is

$$\delta m_e(v) = \left[\frac{m(v)}{\alpha}\right]\left[\frac{F_r}{\langle F(v)\rangle}\right]\left[1 + \frac{F_r}{\langle F(v)\rangle}\right]^{-1}. \quad (4)$$

The modulation excess is computed for the peak of each discernible spectral feature in a given dynamic spectrum. A significant modulation excess ($m_e > 3\,\delta m_e$) denotes variability above radiometer noise.

In the following section, we present two examples of the modulation excess analysis.

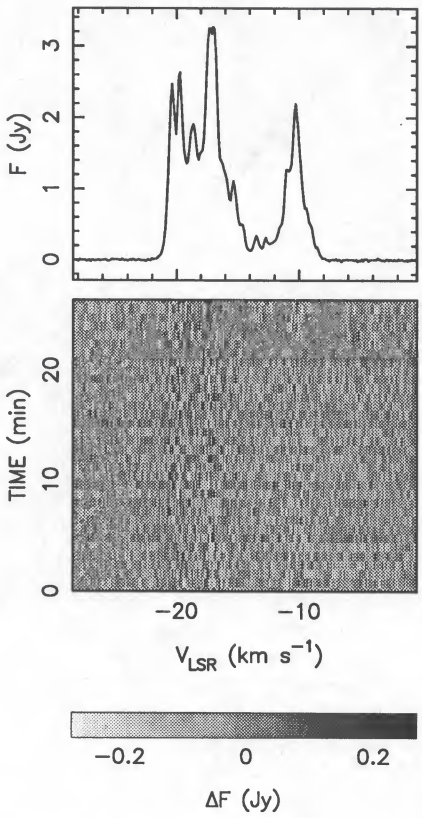

FIG. 1.—Dynamic spectrum of the right circularly polarized emission from the OH/IR maser U Herculis obtained in 1990 March. Shades of gray represent deviation in flux density at a given LSR velocity from its average value during the observation. The absolute scale is shown at the bottom. There is no significant variability above radiometer noise. For convenience, the time-averaged spectrum is reproduced at top with the same velocity axis.

3.1.2. *Examples*

In Figure 1, we display a gray scale representation of the dynamic spectrum of U Herculis in the right-hand polarization. The data were obtained in 1990 March. The modulation index (eq. [1]) was computed for each spectral bin and is plotted in Figure 2 as a function of the mean flux density in the bin, $\langle F(v)\rangle$. Within a section of the spectrum that contains no line emission, the radiometer noise level, αF_r, was determined and used to calculate the expected radiometer-induced modulation index (eq. [2]). The computed values of m_r are shown in Figure 2 as a solid curve. The agreement between $m(v)$ and $m_r(v)$ is excellent. Maximum modulation excesses are $\sim$20% and are consistent within uncertainties with no variability above radiometer noise.

The same analysis is performed for the right circularly polarized spectrum of S269 obtained in 1989 September. The range of flux densities and the amplitude of the radiometer noise in the spectra of S269 and U Her are similar, facilitating a comparison of observed modulation indices. The dynamic spectrum (Fig. 3) suggests that there is significant variability among the 0.5 Jy features near 16 km s^{-1}. Deviations from the radiometer-induced modulation index are evident in Figure 4, confirming the variability seen in the dynamic spectrum. The modulation excesses are not consistent with radiometer noise for these features.

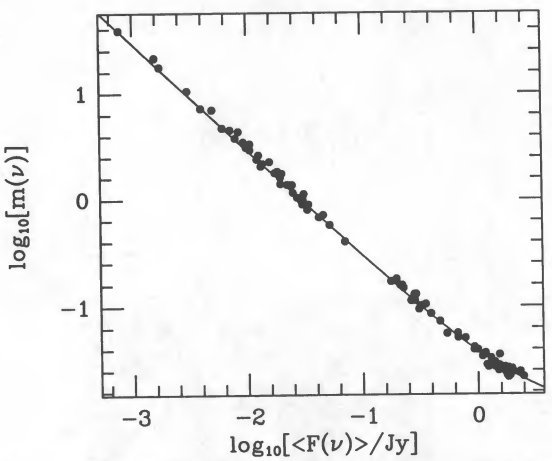

FIG. 2.—Modulation indices $m(\nu)$ (*points*) for each spectral bin ν in dynamic spectrum of U Herculis (Fig. 1) as a function of mean flux density $\langle F(\nu)\rangle$. Curve is the modulation index expected due to radiometer noise (eq. [2]).

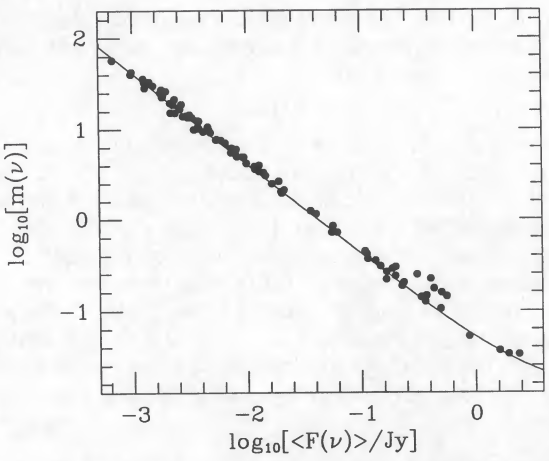

FIG. 4.—Observed modulation indices (*points*) and contribution expected from radiometer noise (*curve*) for S269 data of Fig. 3. The variable features near $V_{LSR} = 16$ km s^{-1} are evident by the systematic offset of modulation indices from the radiometer noise level at $\log(F) \simeq -0.3$.

3.2. *Long Time Scale Variability*

To facilitate comparison of data obtained at different epochs, each dynamic spectrum of a given source is time-averaged to produce a single spectrum. We then compare *relative* amplitudes of the features in the spectra to circumvent uncertainties in absolute flux density calibration.

We believe the multiepoch Arecibo observations provide the most reliable data obtained to date from which to study long-term variability of OH emission. Two or more epochs of data for most sources were obtained using identical hardware (antenna feed, calibration noise diodes, correlator, local oscillators, and frequency mixers) and observing parameters (frequency resolution, LSR velocity origin, and extragalactic

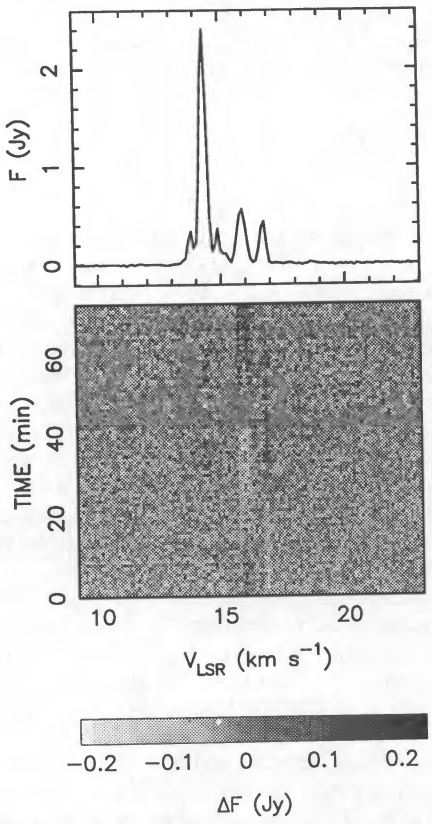

FIG. 3.—Dynamic spectrum of right circularly polarized emission from S269, epoch 4. Gray scale representation is explained in the caption to Fig. 1. Variability is especially evident for the ~0.5 Jy features near $V_{LSR} = 16$ km s^{-1}.

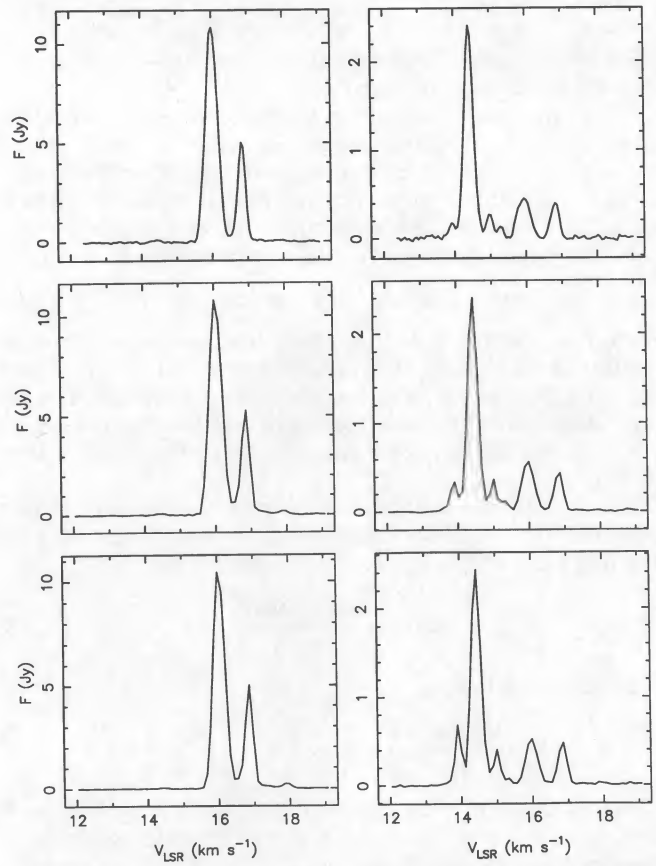

FIG. 5.—The OH spectrum of S269 as it appeared at epochs 2, 4, and 5 (*top to bottom*). As for all figures in this work, the left and right circular polarization spectra appear at the left and right, respectively. The spectra are averages over approximately 2 hr of data.

source calibrators). Where appropriate, we make qualitative comparisons of our Arecibo data with previously published spectra of sufficiently high-velocity resolution.

The single VLA observing epoch can be used in combination with the data obtained by Gaume & Mutel (1987) to provide another reliable base for the study of long-term variability. We employed LSR velocity origins and frequency resolutions in our observations of W49N and NGC 6334F that are compatible with those used by Gaume and Mutel, to facilitate comparison of the data.

4. RESULTS

A source-by-source description of the observational results follows.

4.1. *S269*

S269 is a small Galactic H II cloud and optical bipolar nebula at a distance of 2.0 kpc. Observations of the nebula and associated objects in several wavelength bands have been presented by previous authors (cf. Israel 1976; Wynn-Williams, Becklin, & Neugebauer 1974a; Turner & Terzian 1985). The OH spectrum of S269 as it appeared at epochs 2, 4, and 5 is shown in Figure 5.

Short-term variations with modulation excesses of 20%–80% were evident at all epochs. Figure 6 shows a typical pair of dynamic spectra for this source. There is a brief dip in observed flux density for most features near $t = 20$ minutes. The right-polarized feature at 16.00 km s^{-1} shows a gradual transition from weaker to stronger flux density during the observation, which is not observed to occur for the other features. Gradual brightening or dimming of this feature on time scales of $\sim$20 minutes was noted at each epoch. The time variability of the 16.00 km s^{-1} feature is not mimicked at the corresponding velocity in the left circular polarization at epoch 2. At epochs 4 and 5, the left- and right-polarized time series were roughly complementary, as if a fraction of the emission was being swapped between the two polarizations. We do not know if the two features arise from the same maser spot; our results would suggest that they do. The time series of the 16.88 km s^{-1} feature at each epoch are, in contrast to the 16.00 km s^{-1} emission, similar between the two polarizations rather than complementary. Again, this suggests that the emission in both polarizations arises from the same region.

Over long time scales, the OH emission spectrum is variable. In particular, the 13.91 km s^{-1} feature (RHCP) has been steadily brightening since the first epoch of observation (epoch 2). Its flux density relative to the average of the five remaining bright RHCP features increased nearly fourfold from epoch 2 to epoch 5. At the same time, the right-polarized emission peak at 15.34 km s^{-1} has been steadily dimming. A new LHCP feature appeared between epochs 2 and 4, at 17.98 km s^{-1} (see Fig. 5). The feature remains visible in epoch 5 data and has strengthened.

4.2. *U Herculis*

U Her is a type I (main-line) OH/IR star at a distance of 0.5 kpc and is a Mira variable with an optical period of about 400 days (Engels 1979). Most OH/IR maser models have the emission arising from an expanding circumstellar shell of material. VLBI observations of U Her by Sivagnanam et al. (1988) indi-

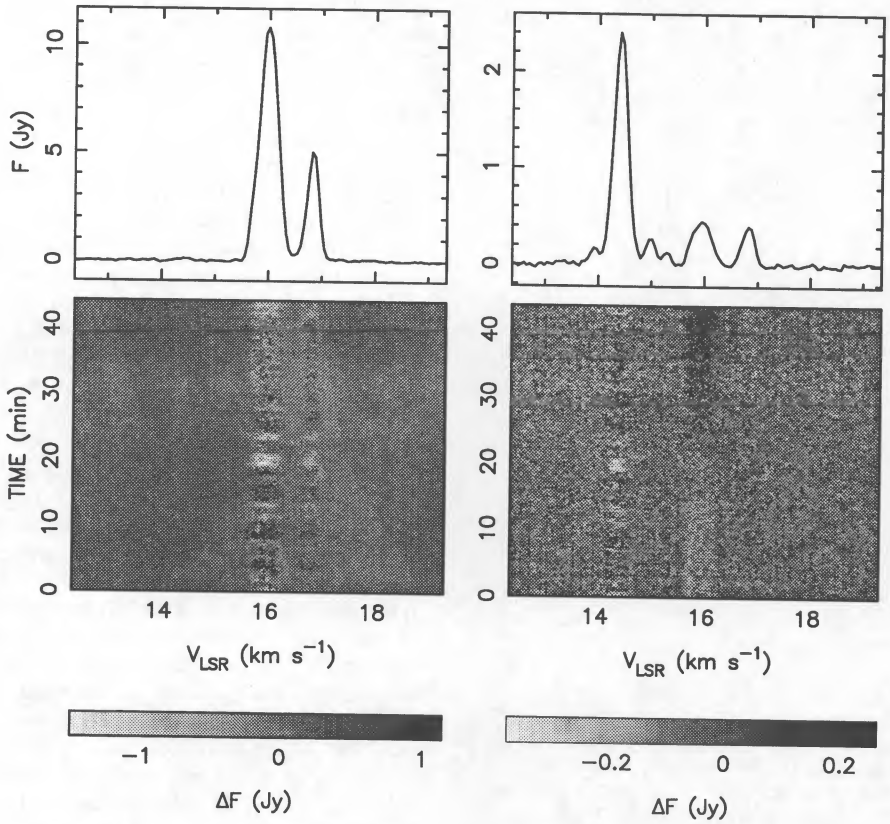

Fig. 6.—Dynamic spectra of the left and right circular polarization emission from S269 (epoch 2)

cate that most of the 1667 MHz OH emission arises from a region larger than 0".1, with the exception of a compact emission source which lies at the blue end of the spectrum. This feature is conceivably an image of the continuum emission from the central star that has been amplified by that part of the OH shell that is expanding directly toward the observer. A Gaussian fit to the *uv* data implies an angular size of 20–25 mas, or about 10 AU, consistent with the expected diameter of a Mira variable. We included U Her in our sample as a control since interstellar scintillation would clearly be quenched for this source, owing to the large angular extent of the emission region.

The emission spectrum of U Her at epochs 1, 2, and 5 is stable, with maximum modulation excesses consistent with little or no variability above radiometer noise. We did not observe significant variability of the most blueshifted component of the spectrum as might be expected if the feature is a scintillating, amplified image of the central star.

The spectrum of U Her is variable on time scales of months (see Fig. 7). A certain degree of variability is expected as a consequence of the variability of the central pumping source and the effects of light travel time across the OH shell. However, we observe long time scale variability beyond a simple oscillation in relative amplitudes of the red- and blueshifted emission peaks.

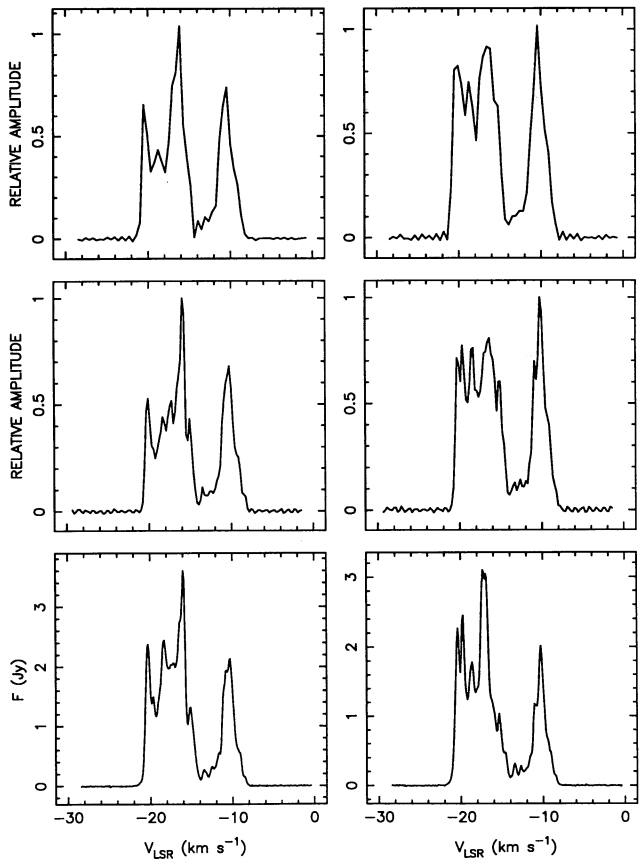

FIG. 7.—Time-averaged spectra of the OH/IR maser source U Herculis at epochs 1, 2, and 5 (*top to bottom*). The epoch 1 data were obtained with 0.22 km s^{-1} resolution; epochs 2 and 5 are 0.11 km s^{-1} resolution. No absolute flux density calibration was performed at epochs 1 and 2. The spectra have been normalized such that the amplitude of the brightest feature is unity (N.B.: the scales are not the same for both polarizations).

Variations between epochs 2 and 5 in the RHCP are especially prominent. Note the brightening of the emission near -17 km s^{-1} with respect to the rest of the spectrum. Significant changes in relative flux density among all the features is evident. Spectra obtained on four consecutive days at epoch 5 do not show significant day-to-day fluctuations. The OH output from U Her at 1665 MHz is not particularly intense and is probably not saturated maser emission. The fluctuations in the shape of the spectrum then reflect exponential amplification of incident radiation. The VLBI results of Sivagnanam et al. support the unsaturated hypothesis, since a saturated maser would not produce an image of the background central star.

4.3. *NGC 6334F*

NGC 6334 is a complex star-forming region whose radio morphology has been studied extensively (cf. Rodríguez, Cantó, & Moran 1982). The region is approximately 1.7 kpc distant (Neckel 1978) and is the closest in our sample of interstellar masers. Our observations are of the maser emission studied by Gaume and Mutel associated with continuum source F. The maser lines arise from a region roughly 2" in extent, with a corresponding linear distance of 34000 AU = 20 lt-days.

We observed NGC 6334F with the VLA (epoch 3). Our average spectra are presented in Figure 8, together with gray scale representations of the dynamic spectra. The emission peak near -8.9 km s^{-1} (LHCP) is significantly variable, with a modulation excess of nearly 600%. The time series of this feature in the LHCP spectrum shows a noiselike variability with rms amplitude of about 3 Jy, superposed upon a steadily increasing component of amplitude $\sim$10 Jy over the duration of the dynamic spectrum. The RHCP feature at -12.2 km s^{-1}, similar in flux density to the -8.9 km s^{-1} LHCP emission, is not as variable (modulation excess $\sim$25%).

The right-polarized emission near -10 km s^{-1} undergoes a brief increase in flux density near $t = 12$ minutes. This behavior is not seen in the other features and is probably not an instrumental effect. There appears to be a strong feature near -13.3 km s^{-1} (RHCP) that is significantly variable; however, it blends with the stronger -12.2 km s^{-1} feature, and no well-defined peak is visible for which to compute a modulation index. This feature is spatially resolved in the survey of Gaume and Mutel, and they list a flux density of 20.2 Jy.

Comparison of the line *shapes* of the individual polarizations to those observed by Gaume and Mutel suggests significant long-term change in the left-polarized spectrum. The ratio of the average fluxes from the LHCP -8.9 and -12.2 km s^{-1} features is $\sim$20.5 in our data and $\sim$34.3 in theirs. If our absolute flux densities are taken at face value, the -12.2 km s^{-1} feature has remained stable at 4.3 Jy, while that at -8.9 km s^{-1} has decreased in flux density by some 60 Jy, from 147 to 87 Jy (see Fig. 9). In any event, the relative amplitudes of the two features have changed significantly. On the other hand, the right-polarized spectrum of Gaume and Mutel agrees in absolute and relative flux densities with our data. The left-polarized -8.9 km s^{-1} feature lies at the phase center of our VLA observations, and is not subject to beam attenuation effects.

Weaver et al. (1968) note marked long-term variability in the spectrum of NGC 6334, with some features changing flux density by as much as one order of magnitude. Furthermore, Robinson, Goss, & Manchester (1970) reported variations in the emission profile at -9 km s^{-1}. In contrast, the data of

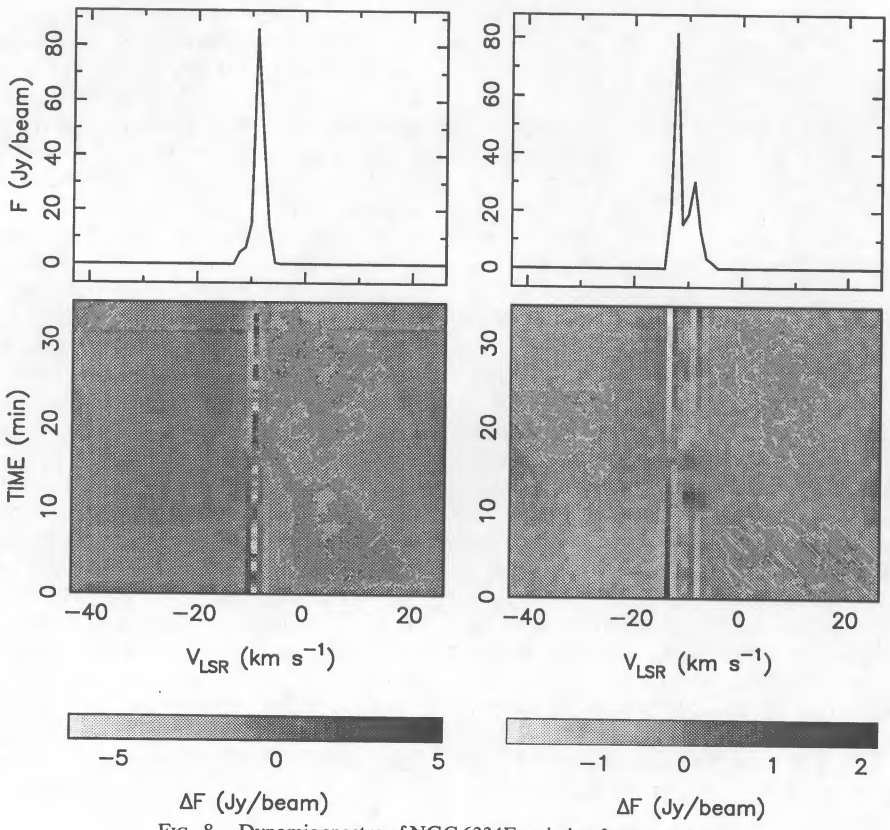

FIG. 8.—Dynamic spectra of NGC 6334F emission from epoch 3

Sullivan & Kerstholt (1976), obtained with a beamwidth of 12′, do not support the existence of any significant variability, although they report a large degree of variability in the OH emission from NGC 6334S, located approximately 15′ to the south. The data are difficult to compare with our own, however, due to the vastly different scale in beamwidths.

4.4. *W49*

W49 is a star forming region approximately 14 kpc distant. Two distinct regions of maser emission are evident (W49N and W49S), separated by approximately 2.′5. Both spectra show intense, multicomponent emission at similar LSR velocities, although the spread in velocity of the northern component is greater. The angular extent of the northern region is approximately 100″ × 10″; however, most maser spots occur within a region 10″ × 10″ in extent. Dynamic spectra of W49N were obtained at epochs 1 and 5; the average spectra are shown in Figure 10. W49S was observed at epoch 5 (Fig. 11).

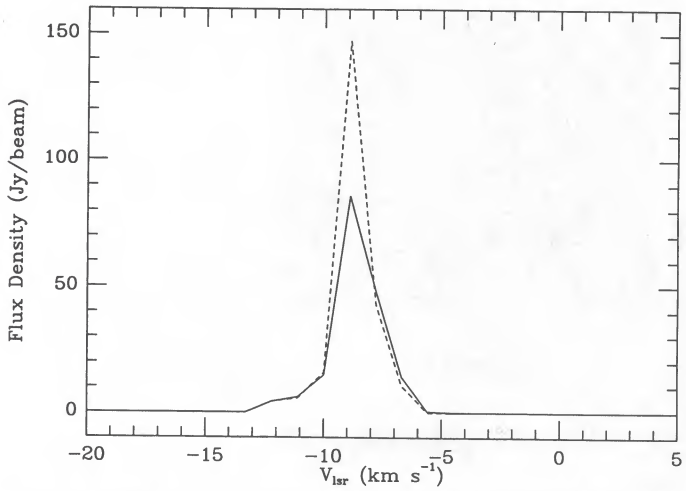

FIG. 9.—Comparison of our VLA spectrum of NGC 6334F, left circular polarization (*solid line*) with that of Gaume & Mutel (1987), obtained in 1985 January (*dashed line*).

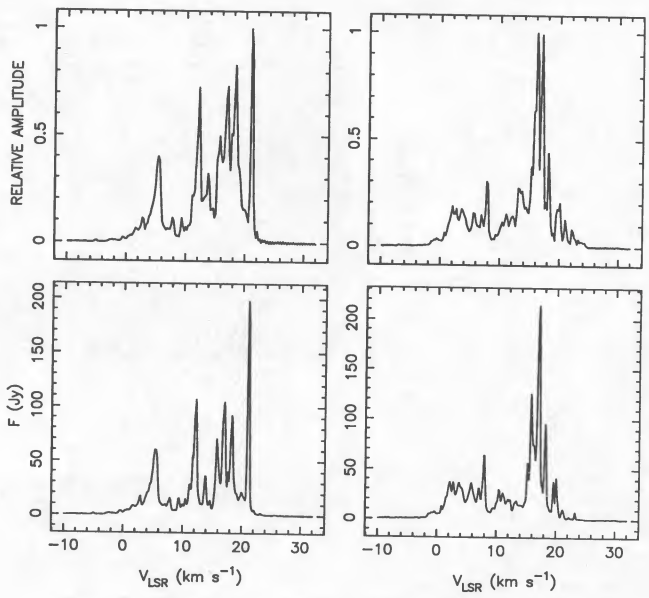

FIG. 10.—Time-averaged spectra of W49N at epochs 1 and 5

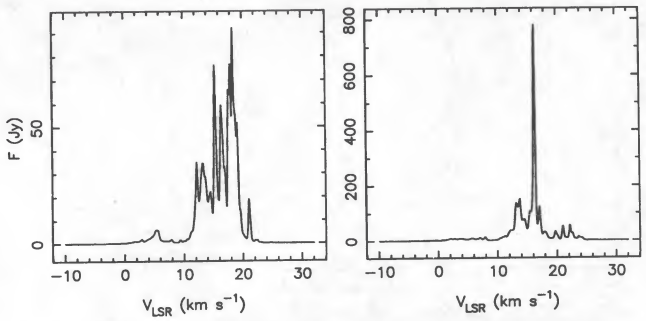

FIG. 11.—Time-averaged spectra of W49S obtained at epoch 5

Analysis of the W49 data from Arecibo is complicated by the existence of the two maser regions separated by approximately one beamwidth (FWHM, ~3′). Both sources are strong emitters in the velocity range 10–20 km s^{-1}, with W49S having a very strong (~800 Jy) feature near 16 km s^{-1}. The sidelobe attenuation between the two sources was estimated at epoch 5 to be approximately 10 dB, based on the amplitude of W49N emission in the velocity range 0 to 10 km s^{-1} present in spectra of W49S, which has no significant emission in this range. Reference to the average spectra of W49N at epochs 1 and 5 (Fig. 10) and W49S (Fig. 11) suggests that the epoch 1 W49N data suffer from significant sidelobe contamination from W49S. The changes in the average spectra of W49N between epochs 1 and 5 are at least partially explained by the difference in sidelobe response to W49S.

Initial inspection of the data suggested extreme variability in the epoch 1 data of W49N, predominantly within the 10–20 km s^{-1} velocity range. In light of the discovery of poor sidelobe suppression of the W49S emission, we are forced to presume that the variability was instrumentally derived. The epoch 5 data show a small degree of variability, with typical modulation excesses of 30%–80%. The W49S data of epoch 5 show a similar degree of excess variability.

Dynamic spectra of W49N were obtained with the VLA at epoch 3. There is no appreciable contamination from W49S; however, the beam is significantly smaller than the total extent of the W49N region. The data of Gaume and Mutel can be used to pinpoint the absolute position of many of the maser features relative to the center of our synthesized beam. We find that most of the bright maser emission falls within the half-power radius of the beam, although caution must be exercised when interpreting the results of our observations.

The dynamic spectra are presented in Figure 12. There is significant variability of many features in both polarizations. Modulation excesses in the right-polarized features are 100%–250%, with the exception of the 14.9 km s^{-1} feature, which has an excess > 1000%. The corresponding bin in the left polarization has a similarly large modulation excess; whether the predominant emission in the two polarizations arises from the same maser spot cannot be ascertained. The time series in the 14.9 km s^{-1} spectral bin is similar in form between the polarizations and is characterized by a gradual reduction in flux density during the observation. The other features in the left-polarized dynamic spectrum possess modulation excesses of ~500% (20.4 and 11.6 km s^{-1}) and ~100% (3.9 km s^{-1}).

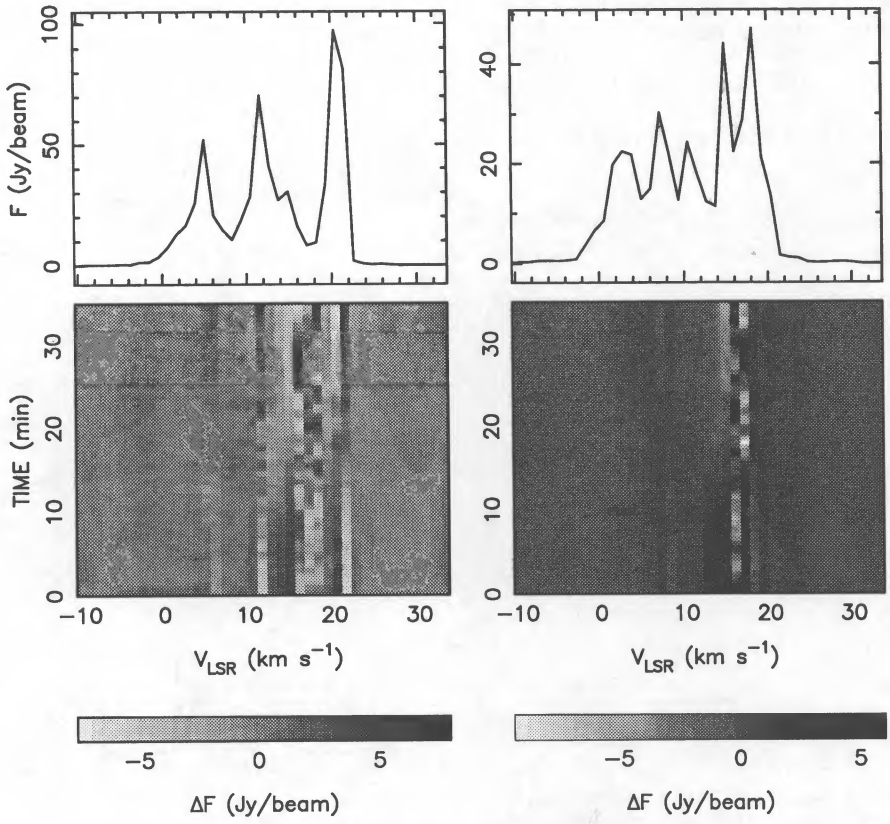

FIG. 12.—Dynamic spectrum of the W49N emission obtained with the VLA at epoch 3

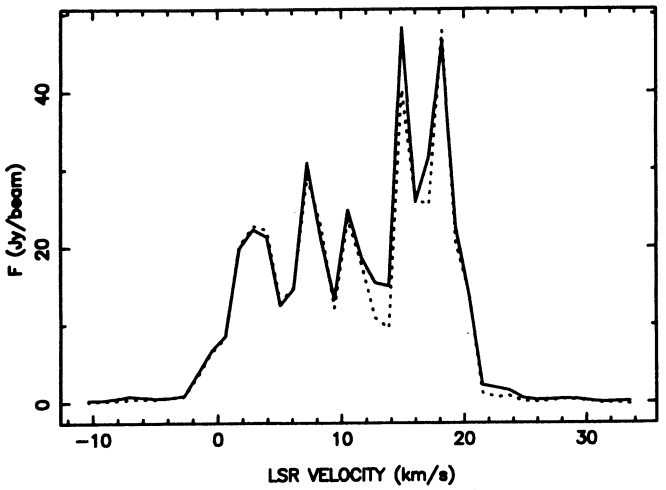

FIG. 13.—Comparison of right-polarized W49N spectra obtained approximately 35 minutes apart. Each spectrum is a single 30 s integration; the solid line is the earlier spectrum.

Figure 13 illustrates the variability seen in the right polarized data. Two spectra separated in time by ~35 minutes have been overlaid. The relative change in amplitude among the features (especially the 14.9 km s^{-1}/18.2 km s^{-1} pair) is evident.

Because of changes in the sidelobe response of the Arecibo system between epochs 1 and 5, the degree of long-term variability in the W49N data is difficult to judge. Excluding the 10–20 km s^{-1} range where sidelobe contamination is a problem, it is evident that the 21 km s^{-1} (LHCP) feature has brightened by ~20% relative to the 5.5 km s^{-1} feature. No changes in the right polarized spectrum outside the 10–20 km s^{-1} range are discernible.

A comparison of our VLA spectra with those of Gaume and Mutel (Figs. 14 and 15) shows a marked reduction in flux density in both polarizations near 17.1 km s^{-1}, between their observing epoch of 1985 January and ours in 1989 May. The excess emission in both polarizations is spatially resolved by Gaume and Mutel and, within positional errors, is probably

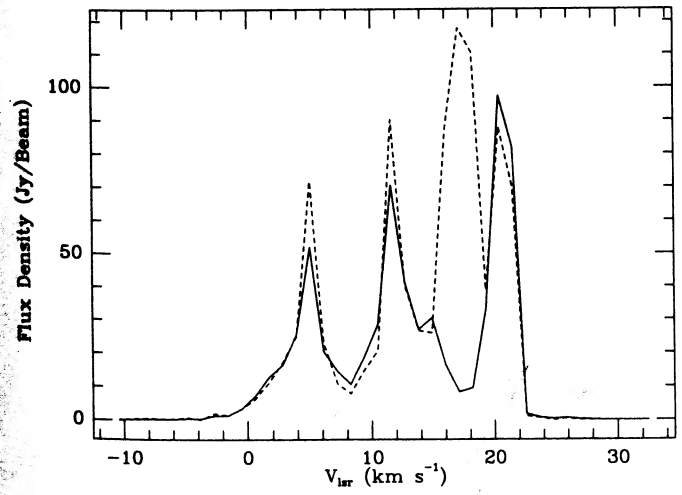

FIG. 14.—Spectrum of W49N (left polarization) obtained by us with the VLA (*solid line*), compared with similar data obtained by Gaume & Mutel (1987) in 1985 January (*dashed line*).

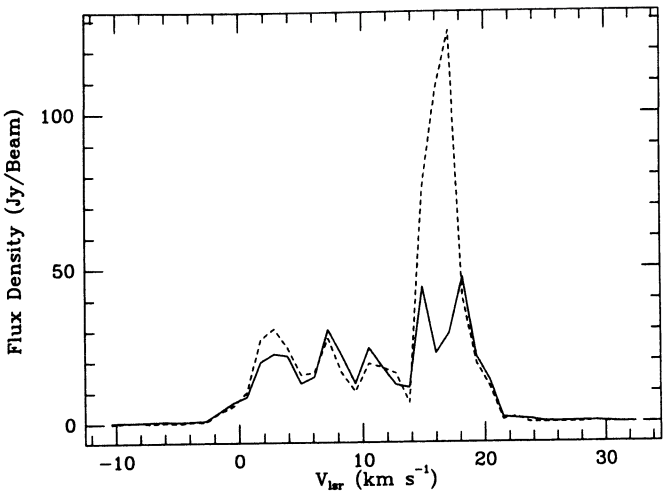

FIG. 15.—Same as Fig. 14, showing changes in right polarization

the same maser spot; it lies approximately 2".4 from the phase center of our data. Smoothing of the Arecibo spectra to match the velocity resolution of the VLA data suggests that the 17.1 km s^{-1} feature is not evident at any of the Arecibo epochs and hence became quiescent at some point between 1985 January and our epoch 1 (1988 April).

It is difficult to compare our results with the variability analyses reported by Sullivan and Kerstholt or Weaver et al., since their beams were much larger and contained the combined emission from the northern and southern components of W49. Sullivan and Kerstholt report that only the relatively dim 22 km s^{-1} feature is variable, while Weaver et al. do not report any significant variability.

Our conclusions for W49 are tentative. There may be short time scale variability, but more detailed observations are required to help isolate sidelobe effects between the two components. Long time scale variability is probable, particularly with regard to the emission near 17.1 km s^{-1} (both polarizations), as well as the 21 km s^{-1} (LHCP) feature.

4.5. *G43.8*

The distance to G43.8 is ambiguous; the recombination line velocity of the associated H II cloud indicates a distance of either 2.7 or 11.8 kpc (Matthews et al. 1978). To our knowledge, no definitive study of this OH maser complex has been published.

We observed G43.8 at epochs 2 and 5. The average spectra are presented in Figure 16. During epoch 2 observations, the emission from G43.8 was moderately variable. The bright, right-polarized peak at 41.54 km s^{-1} showed a modulation excess of ~150%. This peak partially blends with another feature near 41.9 km s^{-1}. The relative amplitudes of these two features remains stable throughout the 40 minute observation.

The epoch 5 data show a significantly greater degree of variability, particularly within the right polarized spectrum. The dynamic spectra are shown in Figure 17. The brightest right polarized feature at 41.65 km s^{-1} decreases in flux density by nearly 15 Jy during the observation, while the blended feature near 41.9 km s^{-1} increases by ~10 Jy in the same period. The modulation excess of the 41.65 km s^{-1} peak is approximately 300%. The left-polarized spectrum is less variable; the bright feature at 41.54 km s^{-1} is most variable, with a modulation excess of 170%.

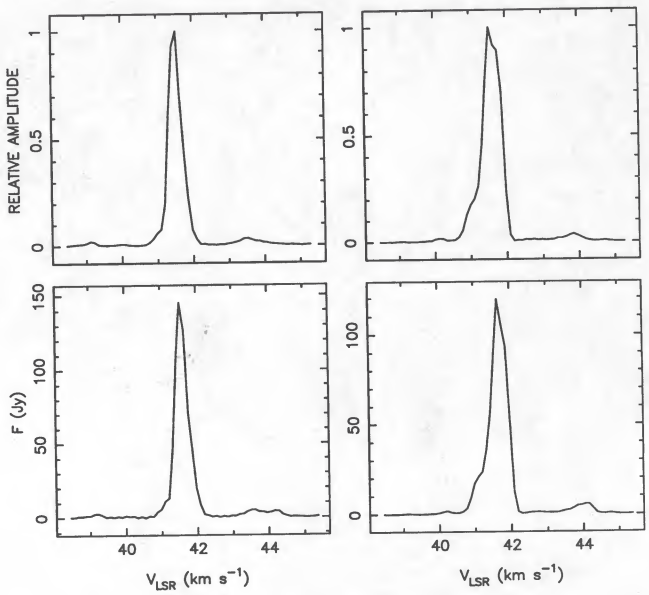

FIG. 16.—Time-averaged spectra of G43.8 at epochs 2 and 5

Long-term variability is evident between the two epochs. The right-polarized emission peak at 41.54 km s^{-1} (epoch 2) has been replaced by the peak at 41.65 km s^{-1} (epoch 5). Inspection of the average spectra (Fig. 16) suggests that the bright emission features in both polarizations are composed of several (>2) narrow components that blend together in velocity space and are variable in relative amplitude between the epochs of observation. The components are intrinsically broader than 0.11 km s^{-1}; increasing the frequency resolution of the spectra did not separate the features. In both polarizations, a new emission component of ~5 Jy flux density has appeared near 44.2 km s^{-1}.

4.6. *G45.5*

G45.5 is a double maser source with component separation of approximately 5′, associated with an H II complex at a distance of approximately 10 kpc. Goss et al. (1973) have mapped the absolute positions and spectra of the two maser groups. The source studied here is the southern component, although the northern maser spot, with emission near 59.4 km s^{-1}, is visible within the sidelobe. The average spectra are reproduced at the top in Figure 18.

To date, G45.5 has been observed at one epoch (epoch 5). At that time, significant variability was identified. The dynamic spectra are presented in Figure 18. The two brightest left-polarized components and the strongest right-polarized feature show similar time series, with periodic brightening and dimming during the observation, and modulation excesses near 200%. The right-polarized feature (~1.7 Jy) at 65.35 km s^{-1} is most variable (modulation excess of 400%) and gradually brightens with time. The 4.8 Jy feature at 66.12 km s^{-1} (RHCP) gradually decreases in flux density; its modulation excess is ~150%. Other features in the spectra show varying degrees of fluctuations. Of particular note is the very stable emission from the 69.74 km s^{-1} peak (RHCP), with no significant variability above radiometer noise.

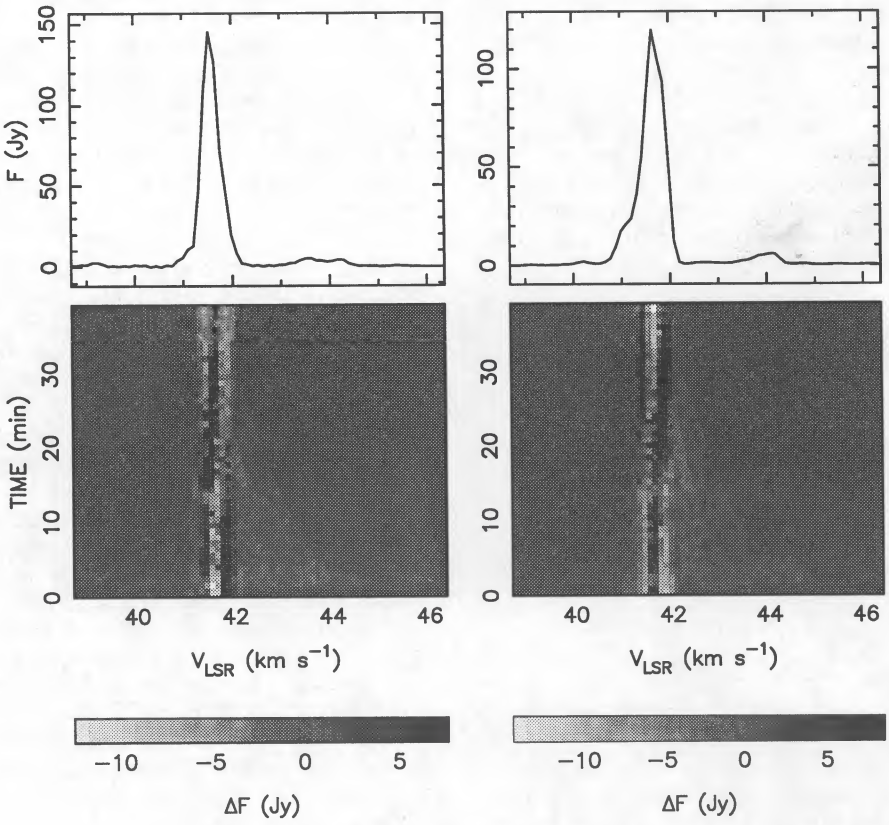

FIG. 17.—Dynamic spectrum of the G43.8 emission at epoch 5

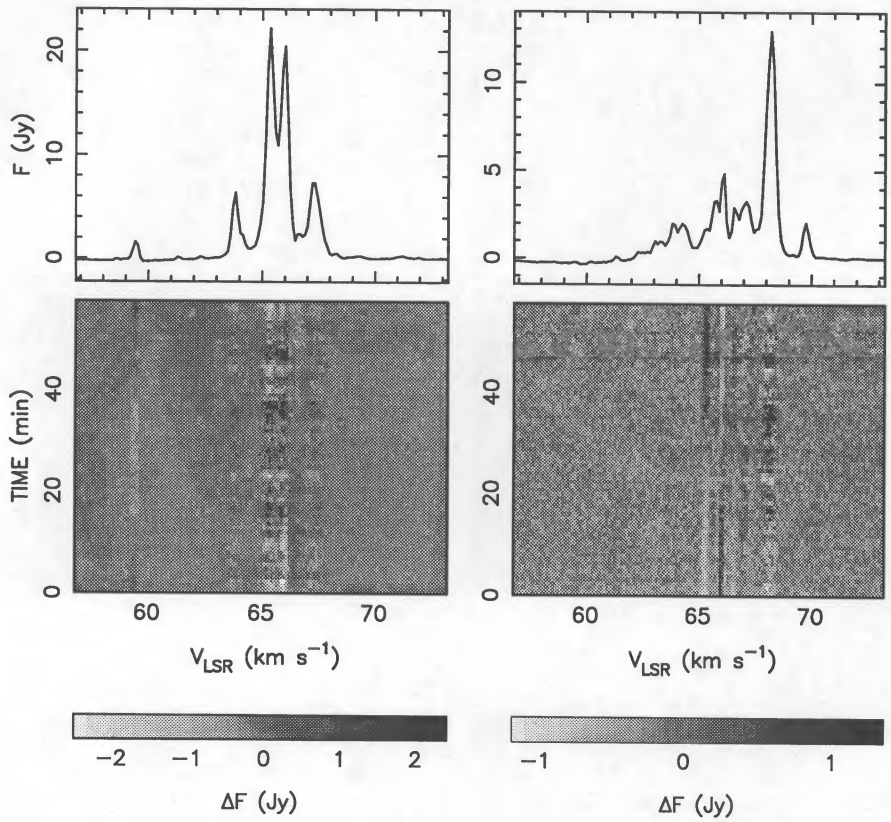

FIG. 18.—Dynamic spectra of G45.5 emission obtained at epoch 5

4.7. *G45.1*

Goss et al. (1973) provide interferometric observations of the OH emission associated with the continuum region G45.1. The masers are localized to two distinct regions separated by approximately 2′. The one studied here is their source OH 45.07+0.13, which lies at a distance of approximately 10 kpc (Wynn-Williams, Downes, & Wilson 1971). The average spectra are shown in Figure 19.

The dynamic spectrum of G45.1 is stable, with maximum modulation excesses of ~50%. This result is consistent with little or no variability above radiometer noise. (Two features in the spectrum at 54.12 and 54.23 km s^{-1} are significantly variable, but are shown in the data of Goss et al. to arise from the maser region 2′ removed from our pointing center. The fluctuations are presumed to be due to sidelobe effects.)

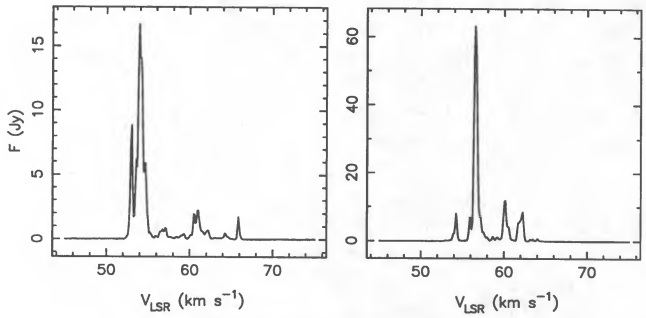

FIG. 19.—Time-averaged specta of G45.1 obtained at epoch 5

4.8. *W51*

W51 is an active star formation site located approximately 7 kpc distant. The maser emission arises from several distinct regions. See Gaume & Mutel for position information. Our VLA observations of W51 include the bright features located near W51 e1 (in the nomenclature adopted by Gaume and Mutel). The Arecibo beam includes W51 e1 and e2, and the weaker emission from masers near W51 IRS 1 and IRS 2, which totals to less than 2 Jy in flux density. The average spectra for epochs 3 and 5 are presented in Figures 20 and 21, respectively.

During VLA observations at epoch 3, the emission peak near 58.0 km s^{-1} was variable in the right and left polarizations (modulation excesses 500% and 250%, respectively). The dynamic spectra are shown in Figure 20. The 58.0 km s^{-1} emission dims with time in the left polarization and brightens in the right. The average spectrum is quite different from that obtained by Gaume and Mutel, so we are not able to ascertain if the emission from the two polarizations arises from the same maser spot. All other features were stable to within the uncertainties.

The data of Gaume and Mutel support the existence of a significant (~1.1 km s^{-1}) shift between left- and right-polarized peaks in the emission from W51 e1. The shift is not present in our data, in which the left and right peaks are coincident within a bin width at 58.0 km s^{-1}.

Epoch 5 observations with Arecibo show several narrow peaks in the left polarization, a single sharp feature in the right polarization, and a broad absorption dip across 60–70 km s^{-1}. It is not known to which maser group (e1, e2, or IRS 1/2) the

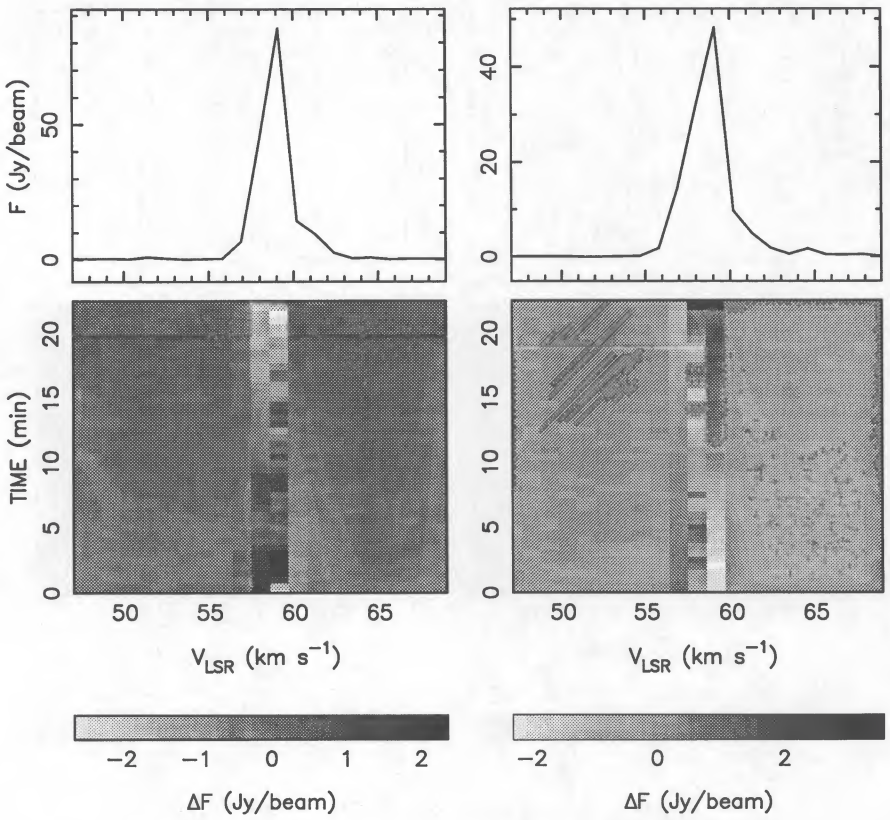

FIG. 20.—Dynamic spectra of W51 e1 obtained with the VLA at epoch 3

individual features belong. No significant short-term fluctuations were noticed in any of the emission features.

Sullivan and Kerstholt report a significant degree of long time scale variability in the 1665 MHz spectra of W51. A qualitative comparison with our Arecibo data suggests that the right-polarized emission peak near 58.33 km s^{-1} has increased dramatically in flux density since 1971, perhaps by a factor of 3 or 4. The feature was only moderately variable in their survey. Our total power spectrum is very different from the one published in Sullivan and Kerstholt, but the differences can be explained by the enhancement of the 58.33 km s^{-1} feature. They do not present separate spectra for the left and right polarizations.

4.9. *ON 1*

ON 1 is a maser complex at a distance of approximately 3.5 kpc. Its OH emission has been observed with the VLA by Ho et al. (1983). The maser spots are spread over an angularly compact region about 2″ in extent, for emission in the 10–20 km s^{-1} range. We also detected low velocity emission near 0–5 km s^{-1} that was outside the bandpass used in the work of Ho et al.

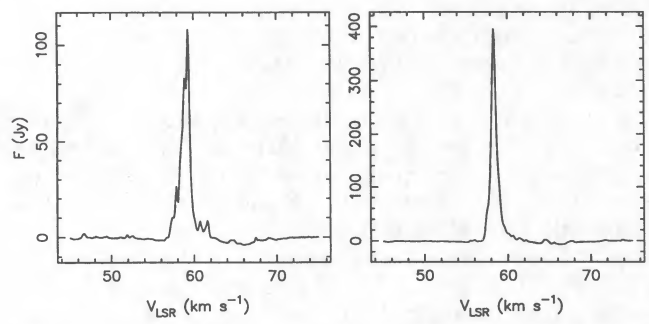

FIG. 21.—Time-averaged spectra of W51 maser complex from epoch 5

ON 1 was observed 3 consecutive days at epoch 1. It did not show any appreciable short time scale variability during that period, nor did the average spectrum change from day to day. In comparison with the other maser sources, ON 1 was unusually stable.

Similar results were obtained at epoch 5. There were no significant short-term or day-to-day fluctuations apparent. Reference to Figure 22 shows that there were substantial changes in the shape of the emission spectrum between the two epochs, particularly with respect to the relative amplitudes of the features in the 11–17 km s^{-1} range. The bright left-polarized feature near 16.2 km s^{-1} has apparently dimmed considerably, although no absolute change in flux density can be determined from the uncalibrated epoch 1 data. A feature at the same velocity in the right-polarized spectrum has also decreased in strength. It is not known if the two features arise from the same maser spot.

The high-velocity OH emission was studied by Winnberg (1970) using the Onsala telescope. It is difficult to reconcile his spectra with ours; many changes have occurred over the 20 years separating the observations. Also, the Onsala spectra have a much lower signal-to-noise ratio than the Arecibo spectra. It is easier to make sense of the comparison if we add $\sim$0.25 km s^{-1} to the cataloged LSR velocities given by Winnberg; we believe there is a systematic difference in LSR velocity computations between the two data sets. (Note that in

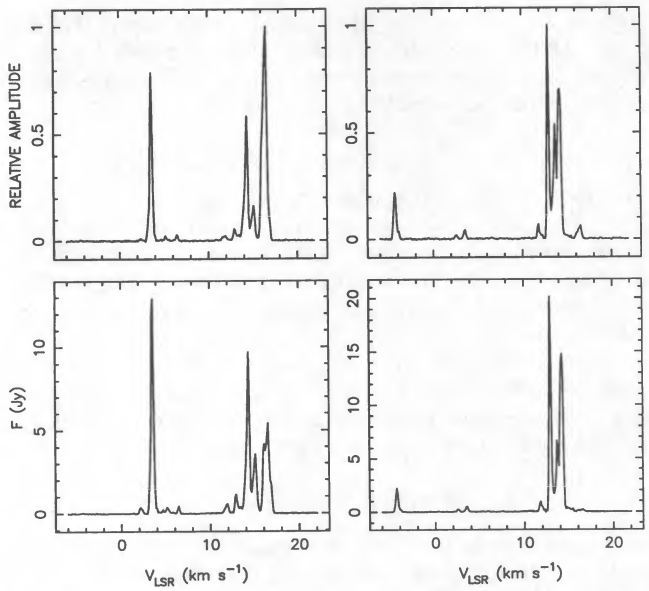

FIG. 22.—Time-averaged spectra of ON 1 observed at epochs 1 (*top*) and 5 (*bottom*).

Winnberg's Table 1, the velocity of the 0.9 K 1665 LHCP feature tabulated in col. [8] should read 14.75 km s^{-1}, not 15.75 km s^{-1}).

Winnberg finds that the brightest right-hand features occur at 12.7, 13.4, and 14.0 km s^{-1}, and have flux densities of 8, 31, and 22 Jy, respectively. Our epoch 5 spectra give 12.90, 13.67, and 14.22 km s^{-1} with flux densities of 20, 7, and 14 Jy. The same comparison for the left polarization gives 16.3, 15.95, 14.75, 14.4 km s^{-1} with 17, 15, 9, and 8 Jy (Winnberg); and 16.52, 16.09, 15.10, and 14.33 km s^{-1} with 5, 4, 4, and 10 Jy (this work). Our 14.33 km s^{-1} LHCP feature does not match with Winnberg's at 14.4 km s^{-1}, when the systematic velocity difference is taken into account; it may be a new or flared feature which masks emission at the expected velocity of ~14.65 km s^{-1}. Winnberg notes that the 12.8 and 13.4 km s^{-1} (his velocities) RHCP emission was variable over the period 1968.8–1970.3.

4.10. *W75S*

The OH maser emission from W75S has been observed by Norris et al. (1982), who also provide accurate positions for the individual spots. The maser complex is spread over ~3″. We adopt a distance of 2.0 kpc to this source, which assumes that W75S is physically related to the nearby complex W75N, whose distance was determined by Dickel, Wendker, & Bieritz (1969). W75S differs from most of the other observed masers in that it is not related to any strong continuum sources.

We observed W75S with the VLA at epoch 3 (Fig. 23). At that time, all features—with one exception—varied significantly on time scales of several minutes. In Figure 23, we plot gray scale representations of the dynamic spectra. The brightest feature (0.9 km s^{-1}) has modulation excesses of 140% and 270% in left and right polarizations, respectively. The 6.4 km s^{-1} feature varies at the 300% level in both spectra, while the 4.2 km s^{-1} feature has excesses of 200% and 500% (left and right). In contrast, the right-polarized feature at −4.6 km s^{-1} is not significantly variable (modulation excess = 30%).

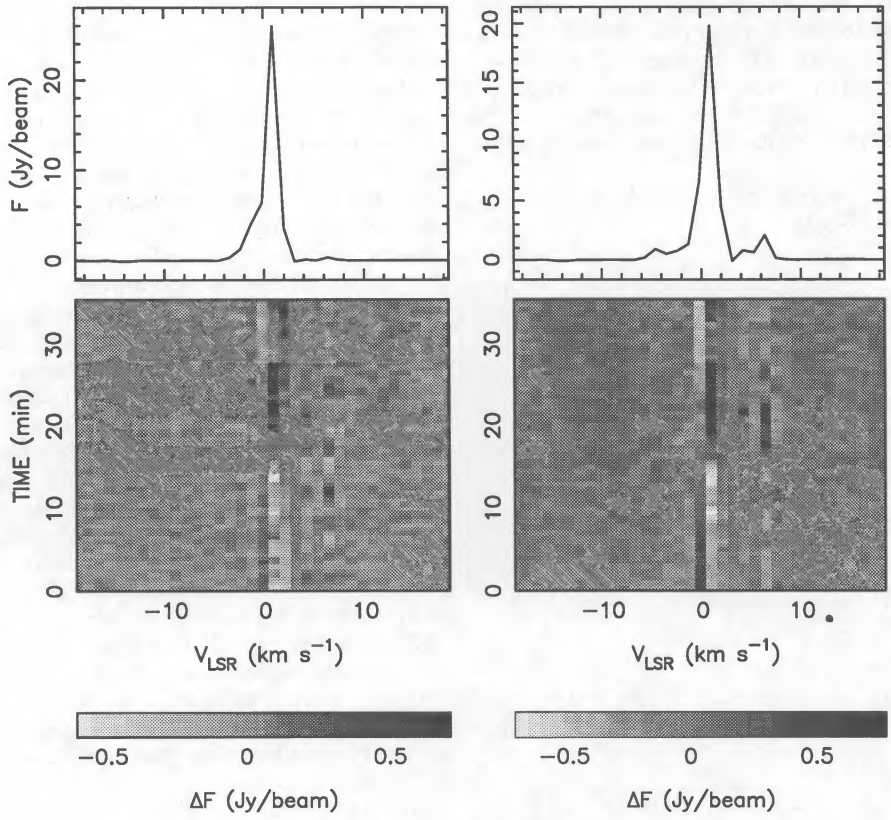

FIG. 23.—Dynamic spectra of epoch 3 W75S emission

The gray scale plots suggest that the right-polarized features show somewhat positively correlated variability (each feature reaches a maximum brightness near $t = 20$ minutes). The exception is the spectral bin at -0.2 km s^{-1}, which contains considerable flux density within the shoulder of the bright 0.9 km s^{-1} feature, and is probably an unresolved emission line. The fluctuations in the left-polarized emission do not appear correlated over frequency. The 0.9 km s^{-1} emission peak shows a similar time series in both polarizations.

Norris et al. (1982) observed considerable long-term variability in the emission at 0.6 km s^{-1} (LHCP) and 1.8 km s^{-1} (RHCP) during the period 1966–1977. The time series of the features were similar, leading to the conclusion that they represent a Zeeman doublet. The resolution of our VLA spectra precludes any conclusion concerning the similarity of fluctuations of the two features on short time scales.

4.11. *Summary of Observations*

To summarize the observational results:

1. Several interstellar masers exhibited spectral fluctuations on time scales as short as minutes.
2. All interstellar masers for which we have multiepoch data showed some degree of variability over time scales of weeks, months, or years.
3. The OH/IR maser was variable on long time scales (months), but was quiescent over time spans of minutes to days.
4. The degree of short time scale variability was itself variable—that is, it depended on the epoch of observation.
5. Time series of short-term fluctuations at a given LSR velocity were not necessarily correlated between the two circular polarizations. If the emission in both polarizations arises from the same maser spot, the sources are variable in both total intensity, as well as percentage circular polarization.
6. There is no obvious correlation in the degree of variability of a given maser feature with distance to the maser complex, total intensity of the feature, line width or LSR velocity.
7. Conceivable instrumental effects have been accounted for.

The degree of short and long time scale variability in each of the sources is summarized in Table 2.

5. DISCUSSION

We have not yet concluded whether the short time scale intensity variations are due to diffractive interstellar scintillation or are intrinsic to the maser/pump systems. Here we discuss the two possibilities, and the constraints each place on the physical dimensions of the masers and the characteristics of the environments in which they exist.

TABLE 2

OCCURRENCE OF VARIABILITY[a]

SOURCE	SHORT TIME SCALE		LONG TIME SCALE
	Arecibo	VLA	
S269	3	...	3
U Her	0	...	3
NGC 6334F	...	3	2
W49N	2	1	3
W49S	2	...	...
G43.8	3	...	3
G45.5	3	...	...
G45.1	0	...	...
W51	0	2	3
ON 1	0	...	3
W75S	...	3	...

[a] Variability classification: (0) not variable; (1) possibly variable; (2) likely variable; (3) definitely variable.

5.1. *Interstellar Scintillation*

A scintillation interpretation places an upper bound on the source size. The fractional intensity modulation of scintillations depends on the ratio of the intrinsic source size to a critical angular size, on the ratio of the observing bandwidth to the diffraction bandwidth, and on the ratio of integration time to the diffraction time scale. We assume this last ratio is less than unity so that the finite integration time does not quench the scintillations. Since a point source observed with a small value of the second ratio has a unit modulation index, the observed modulation index may be written as

$$m_0 = m_{\rm pt} f(\theta/\theta_c) g(\Delta\nu/\Delta\nu_d) , \quad (5)$$

where $m_{\rm pt} = 1$ is the point source modulation index; f and g are functions that decay relatively slowly with their dimensionless arguments and are discussed by Lee (1976), Lerche (1979), and Chashei & Shishov (1976); θ is the true angular diameter of the source while $\theta_c \approx \lambda/D\theta_d$ is a "critical" angular size (with D = source distance and θ_d = scattering diameter). The spectrometer resolution is $\Delta\nu$ while the scintillation (or diffraction) bandwidth is $\Delta\nu_d \approx c/\pi D\theta_d^2$.

Maser observations are probably in the regime $\theta \gg \theta_c$, and often have $\Delta\nu \gg \Delta\nu_d$. Two examples are W49N, which has a VLBI angular diameter (presumably scattering) of $\theta_d \approx 50$ mas and a distance $D \approx 14$ kpc we obtain $\Delta\nu_d \approx 3$ Hz and $\theta_c \approx 10^{-3}$ μas (so long as the dominant scattering material is neither very close to the source nor very close to the observer). For comparison, G45.5 has $\Delta\nu_d \simeq 1500$ Hz and $\theta_c \simeq 10^{-2}$ μas for $D \simeq 9.7$ kpc and $\theta_d \simeq 3$ mas.

The factor g falls off very slowly in its argument, so that the measured modulation index could be obtained even for our spectrometer resolution that is $\times 100$ larger than the diffraction bandwidth. However, the angular factor f is a stronger function of its argument, varying as $f \approx \theta/\theta_c$. To achieve the modulation indices reported here requires that the masers possess intrinsic angular diameters no more than $\sim 10\theta_c$, or a few hundredths of a *micro*arcsecond. For a source of flux density F measured in Jy and intrinsic angular extent θ in μas, the corresponding brightness temperature is $T_b = 1.6 \times 10^{17} F/\theta^2$, and must typically exceed 10^{24} K. To our knowledge, no pumping mechanism or radiative transfer effect that can provide brightness temperatures of this order is viable. Goldreich & Keeley (1972) have shown that under certain circumstances, the observed dimension of the emission region can be as much as two orders of magnitude smaller than the maser proper, but still cannot provide the implied brightness temperature when reasonble physical parameters are assumed.

The ~ 1000 s time scale for variability observed for sources in this survey implies linear scales of approximately one solar radius for transverse line-of-sight velocities of a few tens of km s^{-1} and is consistent with scale sizes of electron density irregularities that drive diffractive modulations of pulsar emission. It is unclear where along the line of sight the scattering occurs, although it is likely that the majority of scattering occurs near to the source, perhaps within the disordered environment surrounding active, high-mass star formation. However, larger critical angular sizes—and lower brightness temperatures—are

derived if the dominant scattering material is much nearer Earth than the maser. In this case, the decorrelation bandwidth, Δv_d, is also greater.

It is expected that scintillating maser line components can show uncorrelated time series between the two circular polarizations because of the often small value for the decorrelation bandwidth for diffractive scintillations (Δv_d), combined with Zeeman splitting of the spectral line. Because our spectral resolution may not be sufficient to resolve either the scintillation bandwidth or Zeeman shifts, we cannot compare time series between polarizations to ascertain the viability of a scintillation interpretation.

To conclude, an interstellar scintillation interpretation of the short time scale variability requires exceedingly large brightness temperatures for the maser emission, particularly if the dominant scattering material is in the vicinity of the maser complex.

5.2. *Intrinsic Short Time Scale Variability*

Intensity fluctuations in laboratory masers and lasers have been observed (cf. Statz & de Mars 1960; Lengyel 1965). In the simplest theoretical model, the maser intensity I and inversion density $n = n_2 - n_1$ (difference in number density of molecules in upper and lower maser states) are described by coupled differential equations (Statz–de Mars equations)

$$\frac{dI}{dt} = nBI - C \tag{6}$$

$$\frac{dn}{dt} = P - nA - 2nBI\,, \tag{7}$$

where A and B are the Einstein coefficients for spontaneous and stimulated transitions between the levels, P is the inversion pump rate, and C is the leak rate of intensity via spontaneous transitions. The solution $I(t)$ is a damped oscillatory function qualitatively linked to a buildup of maser intensity beyond the steady state solution $I(t \rightarrow \infty)$.

The Statz–de Mars equations have been applied to saturated, highly elongated astrophysical OH masers by Salem & Middleton (1978) who predict oscillations in the output intensity with periods ~ 1 day and magnitudes $\lesssim 25\%$ using reasonable physical parameters. Their intensity curves are the response of the maser to the sudden onset of a pumping mechanism, and the 25% oscillations are observed after an initial flare ($\lesssim 1$ order of magnitude) subsequent to pump turn-on. Realistically, astrophysical masers are likely responding to a series of pump disturbances, and their light curves are therefore a complicated sum of damped oscillations with various time lags.

The oscillation period is the light travel time across the length of the maser and is also an upper limit to the length of time required for a pump disturbance to propagate through the maser. Various models are possible, but the shortest oscillation period follows from radiative or collisional disturbances propagating across the short dimension of the elongated maser. For the observed variations of duration $\gtrsim 10$ minutes, the light travel distance is $\gtrsim 1$ AU, and implies a brightness temperature T_m approaching 10^{15} K. For a collisional disturbance propagating with velocity ~ 10 km s^{-1} across the maser, the short dimension is $\sim 10^{-3}$ AU, with an exceedingly large implied brightness temperature of 10^{20} K. In this case, the observed angular size is ~ 1 μas, and some degree of scintillation would likely be evident for the more weakly scattered masers.

The light curves of most of the individual maser features observed in this survey are conceivably incomplete segments of oscillations occurring over time scales longer than the observing period of 1–2 hr. The required brightness temperatures are reduced if the oscillations in the intensity curves have significantly longer periods of, for example, 24 hr. For collisional and radiative pump disturbances over these time scales, the required brightness temperatures are reduced from the above estimates by a factor $\sim 2 \times 10^4$, to $\sim 5 \times 10^{15}$ K for collisional processes and $\sim 5 \times 10^{10}$ K for radiative disturbances. For comparison, Elitzur (1987) derives T_m for a maser pumped by a blackbody of temperature T_p subtending a solid angle Ω_p as viewed at the maser,

$$T_m = \eta T_p (\nu_p/\nu_m)^2 (\Omega_p/\Omega_m)\,, \tag{8}$$

where η is the efficiency of converting pump photons of frequency ν_p to maser photons of frequency ν_m, and Ω_m is the solid angle of the maser emission. Equation (8) assumes the pumping is through a spectral line of similar fractional bandwidth to the maser line. A brightness temperature $T_m \simeq 0.5 \times 10^{10}$ K is derived if the OH maser is pumped through the 35 μm rotational transition by IR emission with $T_p = 500$ K, if one assumes, for example, $\Omega_p \simeq \Omega_m$ and $\eta = 0.5$. The result is about one order of magnitude below the figure required for oscillatory intensity fluctuations of period ~ 1 day, keeping in mind that a number of parameters are poorly constrained (e.g., Ω_p, Ω_m, η). The temporal structure of the intensity variations beyond the ~ 1–2 hr duration of the dynamic spectra is not known; it would be instructive to obtain continuous light curves over considerably longer time spans.

Alternative methods of inducing short time scale variability have been described in the literature. For example, some authors have discussed models in which electron or ion streaming motions arise near the ionization and shock fronts of the expanding H II region (cf. Elitzur 1979; Johnston 1967; Evans et al. 1979). The anisotropic velocity distribution is able to maintain population inversions which can in many cases provide the observed maser luminosities. However, the models are derived for maser spot sizes of typically 100–1000 AU, and when combined with our variability observations would require characteristic bulk velocities orders of magnitude greater than the sonic velocity. Recently, Elitzur (1990) has suggested that disturbances in the maser level populations can produce intensity fluctuations. Fluctuations in the inversion density over small path lengths in the unsaturated maser core can evidently give rise to significant intensity modulations with characteristic time scales $\sim 1/\Lambda$, where Λ is the loss rate of molecules from the masing levels. This description is a potential explanation for variability on minute-like time scales, although further study is needed.

5.3. *Long Time Scale Variability*

Gwinn et al. (1988) have searched for and not found refractive wandering of water masers in the Sgr B2(N) complex. The result, when combined with observed (presumably scattered) spot sizes, either bounds the slope of the wavenumber spectrum of electron density turbulence (shallower than, or approximately equal to, the Kolmogorov value), or implies a cutoff in large-scale electron density irregularities at approximately 1 AU.

The time scale expected for refraction effects can be estimated for turbulent spectra with power-law indices $\lesssim$ the Kolmogorov value as $\tau_r \simeq \theta_d D/v$, where v is the velocity of the refracting screen perpendicular to the line of sight. For masers in our sample for which θ_d is known, τ_r varies from 3 to 300 yr, assuming $v = 10$ km s^{-1}.

The results of Gwinn et al., and the implied time scale for refraction, suggests that the long time scale modulations of the maser spectra (which can approach 100%) are not refraction phenomena. Instead, we favor a model in which the variations on time scales of weeks to years are intrinsic to the masers. The fluctuation times do not significantly constrain the linear dimensions of the masers or their pumping source: 0.2 AU and 5000 AU for sonic (10 km s^{-1}) and speed of light travel distances, respectively, over 30 days time.

OH emission from the type I (main-line) OH/IR star U Her is not particularly strong, and the maser may not be saturated. In this regime, it is not surprising that the relative strengths of features in the spectrum change on long time scales since the maser is responding exponentially to the input radiation, and small changes in the intensity of background 18 cm radiation produce disproportionately large fluctuations in the output.

6. CONCLUSIONS

Emission spectra of eight of 10 interstellar masers are variable on time scales as short as *minutes*. The characteristics of the fluctuations are summarized in § 4.11. We cannot presently pinpoint the origin of the variability, although instrumental effects are unlikely. An interstellar scintillation interpretation is complementary to previous observations which suggest that the angular size of the maser spots follow a scaling law in wavelength consistent with scattering by electron density turbulence in the ISM. In this model, however, exceedingly high brightness temperatures (10^{24} K) are required. Intrinsic variability is possible, and several viable methods of imparting the fluctuations are found in the literature. Brightness temperatures consistent with radiative pump models (that is, $\lesssim 10^{10}$ K) are obtained if the observed fluctuations are segments of quasi-periodic variability that occur over somewhat longer time scales of ~ 24 hr and are produced by the response of the maser to pump disturbances (Salem & Middleton 1978). Alternatively, Elitzur (1990) has shown that variations can be imparted on time scales $\sim 10^3$ s by variations in the maser inversion density along the ray path in the unsaturated maser core.

All interstellar masers for which multiepoch observations are available exhibit significant spectral fluctuations on longer time scales of weeks, months, or years. These changes are likely intrinsic to the masers and are perhaps related to the dynamics of the regions in which the masers are embedded. The OH/IR source also exhibited long time scale variability in the detailed shape of its spectrum. Its emission—not particularly intense—may arise from an unsaturated maser, and the fluctuations a consequence of the exponential response to input 18 cm radiation of varying strength.

The authors have benefited from discussions with Willem Baan, Mike Davis, Moshe Elitzur, Ralph Gaume, Carl Gwinn, Jim Moran, and Mark Reid. This research was sponsored by the National Science Foundation under grant AST 85-20530.

APPENDIX

INSTRUMENTAL EFFECTS

A variety of instrumental effects impart variability in the dynamic spectra on short timescales and require identification and/or elimination.

1. ZENITH ANGLE EFFECTS AT ARECIBO

The Arecibo system is subject to zenith angle variations in telescope gain and noise temperature because of the changing illumination pattern of the suspended feed upon the dish. At large zenith angles [(ZA) greater than $\sim 10°$], the illumination pattern includes the surrounding terrain, and a reduction in gain and increase in system temperature is produced. Our observations were limited to ZA $< 10°$, where these quantities are constant to within approximately 3%. We would expect time series of flux densities from different velocity components of a given source to be "in phase" with one another if the telescope gain was varying uniformly across the band. This was not the case. To explain our results, the gain would have to be changing nonuniformly across the band at a level comparable in magnitude to the observed modulation indices—an effect which to our knowledge has not been reported by previous Arecibo observers. Also, the OH/IR maser does not fluctuate significantly, even though it would have been affected by the same gain changes. Last, the gain of the telescope decreases with ZA, yet some line components show a marked *increase* in flux density with increasing ZA.

2. POINTING ERRORS

2.1. *Arecibo*

Our experience suggests that the Arecibo system is subject to significant pointing errors due to various influences including precipitation, thermal stress and relaxation of the feed support structure, and torques generated by tracking motions of the suspended feeds. The pointing offsets have produced gain changes as large as 5% in the dynamic spectra.

Problems of this type are straightforward to identify. They are often manifest as repeatable, zenith angle-dependent gain changes that, due to the compact sizes of the maser regions with respect to the beam diameter, affect all line components similarly. Fluctuations with such characteristics have been presumed instrumental in origin, and discounted.

2.2. VLA

The pointing accuracy of the synthesized VLA beam is a function of the phase stability among the individual array elements during the observation. Time dependent phase corrections are applied to the *uv* data based on periodic observations of calibrator sources. Phase stability of the array is generally of concern only at high frequencies in the A configuration (the largest), where atmospheric and ionospheric effects become important. At the 18 cm OH frequency with a B/C hybrid configuration, we observed nominal phase stability throughout the observations, and believe that the pointing accuracy of the array was good to a small fraction of the beam size.

3. BEAM ROTATION

3.1. *Arecibo*

Small scale diffraction structure in the beam response of the observing system, when combined with parallactic angle rotation, imparts variability in the dynamic spectra. The effect is seen as zenith angle–dependent gain changes that, depending on the angular extent of the maser complex, may not be uniform across the spectrum. In a single observation, variability imparted by beam rotation is difficult to identify; repeated observations of the same source will reveal similar flux densities as functions of zenith angle for the different velocity features.

The effect is not apparent at the few percent level in the Arecibo data. Several line components in the W49N spectra whose relative positions are discernible from the interferometric data of Gaume and Mutel do not show relative, zenith angle–dependent fluctuations when observed repeatedly over several days. The results suggest that the Arecibo beam does not possess azimuthal distortions at levels greater than $\sim 5\%$ over 30″ angular scales.

3.2. *VLA*

The lack of multiepoch VLA data makes it difficult to ascertain the effects of time-variable *uv* coverage on the dynamic spectra of the maser sources. For sources W51 e1, NGC 6334F, and W75S, previous interferometric observations show that the bright emission components fall well within our VLA synthesized beam. Asymmetries in the beam response are unlikely to produce the observed $\sim 10\%$ fluctuations. For the extended maser source W49N, the effect of finite beam coverage across the complex may impart significant fluctuations in the observed emission profile. The amplitude and extent of the instrumental fluctuations are not known; this source requires additional study.

4. SIDELOBE CONTAMINATION

Several molecular regions possess multiple complexes of strong maser emission (e.g., W51, W49, G45.5, G45.1). The potential exists for substantial variability imparted by sidelobe responses to nearby maser emission. In all of the cases studied here, the multiple nature of the maser complexes has been studied previously by other authors, and the results used in this survey to identify the instances of possible sidelobe contamination. We have succeeded in identifying sidelobe-induced variability in the sources listed above, and have disregarded those features that are affected. Furthermore, Arecibo observations have been made one beamwidth (3′) offset from all of the masers within the Arecibo declination range, in each of eight directions (N, NW, W, SW, etc.) to survey for possible sources of contaminating emission; no previously unobserved emission was found.

5. BINNING EFFECTS

We do not believe that the fluctuations are related to drifting of the spectral features through the nonuniform response of the FFT across frequency (the so-called "picket fence" effect). This phenomenon was modeled using a contrived spectral line. The result is that significant modulations ($m \sim 10\%$) in the line intensity will result only if the line drifts completely through one or more bins during the observation. Our velocity correction routine (mentioned in § 2) prevents such an occurrence. Furthermore, data at epochs 3, 4, and 5 were corrected in real time for LSR acceleration, and therefore should not be subject to such an effect.

6. CORRELATOR EFFECTS

At the beginning of each dynamic spectrum, optimum digital threshold levels for three-level sampling were set by the hardware, based on in-line power counters. Therefore, the thresholds were not changed until a new dynamic spectrum was begun. Incorrect threshold settings may result as the system temperature changes throughout the observation, which would cause variability in the signal level of the resultant power spectra. However, we believe that this effect is not present for two reasons. First, most system temperatures were dominated by the maser emission itself, so that variability in the maser strength is required to necessitate changes in the threshold settings. The observed level of total power variability in the maser emission is not sufficient to cause serious errors in the threshold settings. Second, such an effect cannot produce frequency-dependent changes in signal level, but will affect all line components similarly.

7. TYPES OF VARIABILITY SEEN

We have compiled the following partial list of observed behavior in the spectra, toward the goal of establishing that no unknown or untested systematic effects can consistently explain all of the short time scale variability. Only Arecibo dynamic spectra are discussed, due to the limited amount of VLA data obtained in one epoch of observing. However, most of the phenomena discussed below are also found in the VLA spectra.

1. *Relatively dim source with little or no variability.*—Rules out a broad range of instrumental effects. Example is the OH/IR star U Her, at all epochs of observation. Peak flux density is ~ 3 Jy, per polarization; no line components are significantly variable. Interstellar maser example is ON 1, which is also quiescent at all epochs.

2. *Relatively bright source with little or no variability.*—Rules out a broad range of instrumental effects, including dynamic range limitations. Example is W51, epoch 5 data (Arecibo). Peak flux density is 110 Jy (LHCP) and 400 Jy (RHCP). The right-polarized peak represents a $\sim$90 times enhancement of system temperature over the off-line value. No features in the spectrum (down to the dimmest, $\sim$1 Jy peaks) exhibit significant modulation excess.

3. *Relatively dim source exhibiting variability.*—Contrast with item (1) above. Example is G45.5, epoch 5. Brightest features are approximately 22 and 13 Jy (LHCP, RHCP). Modulation excesses of 200% noted in both polarizations for many features.

4. *Relatively bright source exhibiting variability.*—Contrast with item (2) above. Example is G43.8, epoch 5. Maximum flux densities are 150 (LHCP) and 120 (RHCP) Jy, with respective modulation excesses of 170 and 300%.

5. *Spectra with brighter features more variable than weaker ones.*—Constrains, among other things, the effect of "sidelobe" response from bright, sharp spectral features on dimmer ones. Example: G43.8 epoch 5. Modulation excesses (170%–300%) of bright (120–150 Jy) features near 41.6 km s^{-1} are significantly greater than those for dimmer features near 44 km s^{-1} (excesses $<$100%).

6. *Spectra with dimmer features more variable than brighter ones.*—Dynamic range limitations are likely to exhibit the opposite behavior. G45.5 RHCP epoch 5. Most variable feature is 1.7 Jy line at 65.35 km s^{-1} (excess of 400%), while brightest features (12–22 Jy) are less variable (excesses $\sim$200%).

7. *Degree of variability in both polarizations roughly equal.*—Argues against polarization-dependent systematic effects. Example is S269 at all epochs, with modulation excesses as great as $\sim$80% in both polarizations.

8. *RHCP spectra with significantly greater variability than LHCP.*—See G43.8 epoch 5. RHCP peak (120 Jy) has 300% excess, LHCP peak (150 Jy) about 170%.

9. *LHCP spectra with significantly greater variability than RHCP.*—No rigorous examples. However, there are many cases of approximately equal variability (item [7]), including cases with left-polarized variability as great as 500% (e.g., some of the W49N features outside of the range of LSR velocities possibly contaminated by W49S).

10. *All features variable in a given spectrum.*—Significant variability regardless of flux density. Example is S269, both polarizations, all epochs of observation.

11. *Spectrum with some features variable, others not.*—Good example is the very stable emission from the 69.74 km s^{-1} RHCP feature (2 Jy) of G45.5 epoch 5, while, for example, the 65.35 km s^{-1} feature in the same spectrum (with similar flux density, $\sim$1.7 Jy) possesses significant variability (modulation excess of 400%).

REFERENCES

Bowers, P. F., Reid, M. J., Johnston, K. J., Spencer, J. H., & Moran, J. M. 1980, ApJ, 242, 1088
Boyd, R. W., & Werner, M. W. 1972, ApJ, 174, L137
Burke, B. F., et al. 1968, AJ, 73, S168
Chashei, I. V., & Shishov, V. I. 1976, Soviet Astr., 20, 1
Diamond, P. J., Martinson, A., Dennison, B., Booth, R. S., & Winnberg, A. 1988, in Radio Wave Scattering in the Interstellar Medium, ed. J. Cordes, B. Rickett, & D. Backer (New York: AIP), p. 195
Dickel, H. R., Wendker, H. J., & Bieritz, J. H. 1969, A&A, 1, 270
Elitzur, M. 1979, A&A, 73, 322
———. 1987, in Interstellar Processes, ed. D. J. Hollenbach & H. A. Thronson, Jr. (Dordrecht: Reidel), p. 772
———. 1990, private communication.
Engels, D. 1979, A&AS, 36, 337
Evans, N. J., II, Beckwith, S., Brown, R. L., & Gilmore, W. 1979, ApJ, 227, 450
Gaume, R. A., & Mutel, R. L. 1987, ApJS, 65, 193
Goldreich, P., & Keeley, D. A. 1972, ApJ, 174, 517
Gómez Balboa, A. M., & Lépine, J. R. D. 1986, A&A, 159, 166
Goss, W. M., Lockhart, I. A., Fomalont, E. B., & Hardebeck, E. G. 1973, ApJ, 183, 843
Gwinn, C. R., Moran, J. M., Reid, M. J., & Schneps, M. H. 1988, ApJ, 330, 817
Habing, H. J., Goss, W. M., Matthews, H. E., & Winnberg, A. 1974, A&A, 35, 1
Hagen, J. B., & Farley, D. T. 1973, Rad. Sci., 8, 775
Hardebeck, E. G. 1972, ApJ, 172, 583
Ho, P. T., Haschick, A. D., Vogel, S. N., & Wright, C. H. 1983, ApJ, 265, 295
Israel, F. P. 1976, A&A, 52, 175
Johnston, I. D. 1967, ApJ, 150, 33
Lee, L. C. 1976, ApJ, 206, 744
Lengyel, B. A. 1965, Introduction to Laser Physics (NY: John Wiley and Sons)
Lerche, I. 1979, ApJ, 234, 653
Matthews, H. E., Shaver, P. A., Goss, W. M., & Habing, H. J. 1978, A&A, 63, 307
Mezger, P., & Höglund, A. 1967, ApJ, 147, 490
Napier, P. J., & Crane, P. C. 1982, in Synthesis Mapping, ed. A. R. Thompson & L. R. D'Addario (Green Bank: National Radio Astronomy Observatory), p. 3–1
Neckel, T. 1978, A&A, 69, 51
Norris, R. P., Booth, R. S., Diamond, P., & Porter, N. D. 1982, MNRAS, 201, 191
Perley, R. A. 1982, AJ, 87, 859
Reid, M. J., & Moran, J. M. 1988, in Galactic and Extragalactic Radio Astronomy, ed. G. L. Verschuur & K. I. Kellerman (New York: Springer), p. 255
Rickett, B. 1990, ARA&A, 28, 561
Robinson, B. J., Goss, W. M., & Manchester, R. N. 1970, Australian J. Phys., 23, 363
Rodríguez, L. F., Cantó, J., & Moran, J. M. 1982, ApJ, 255, 103
Rots, A. H. 1982, in Synthesis Mapping, ed. A. R. Thompson & L. R. D'Addario (Green Bank: National Radio Astronomy Observatory), p. 8–1
Salem, M., & Middleton, M. S. 1978, MNRAS, 183, 491
Sivagnanam, P., Diamond, P. J., Le Squeren, A. M., Daigne, G., Biraud, F., Ortega-Molina, A., & Graham, D. A. 1988, A&A, 194, 157
Statz, H., & de Mars, G. 1960, in Quantum Electronics (New York: Columbia University Press), p. 530
Sullivan, W. T., & Kerstholt, J. H. 1976, A&A, 51, 427
Turner, B. E. 1971, Ap. Letters, 8, 73
Turner, K. C., & Terzian, Y. 1985, AJ, 90, 59
Weaver, H., Dieter, N. H., & Williams, D. R. W. 1968, ApJS, 16, 219
Winnberg, A. 1970, A&A, 9, 259
Wynn-Williams, C. G., Becklin, E. E., & Neugebauer, G. 1974a, ApJ, 187, 473
Wynn-Williams, C. G., Downes, D., & Wilson, T. L. 1971, Ap. Letters, 9, 113
Wynn-Williams, C. G., Werner, M. W., & Wilson, W. J. 1974b, ApJ, 187, 41